

Evidence for Intensification of North Pacific Winter Cyclones since 1948



Nicholas E. Graham*⁺ and Henry F. Diaz[#]

ABSTRACT

Using NCEP–NCAR reanalysis and in situ data, evidence of important changes in the winter (December–March) cyclone climatology of the North Pacific Ocean over the past 50 years is found. The frequency and intensity of extreme cyclones has increased markedly, with associated upward trends in extreme surface winds between 25° and 40°N and major changes in cyclone-related circulation patterns in the Gulf of Alaska. Related increases in extreme wave heights are inferred from wave measurements and wave-model hindcast results. The more vigorous cyclone activity has apparently resulted from increasing upper-tropospheric winds and vertical wind shear over the central North Pacific. Such changes, which create an environment more favorable for cyclone formation and intensification, may be related to the observed modulation of El Niño–related teleconnections at decadal and longer timescales. It is intriguing that this trend has been relatively steady rather than the sudden or stepwise shifts documented for other aspects of North Pacific climate change. Increasing sea surface temperatures in the western tropical Pacific are suggested as a plausible cause of the observed changes, though other underlying mechanisms may also contribute.

1. Introduction

Much research during the past few decades has focused on the character and causes of variability in the time-averaged circulation over the North Pacific Ocean. Although the timescales range from seasons to decades and details of the spatial patterns vary, most analyses reveal a dominant mode associated with fluctuations in the strength, position, and extent of the Aleutian low. Many studies indicate that much of this variability is related to changes in tropical Pacific sea surface temperatures (SSTs; e.g., Bjerknes 1966; Hoskins and Karoly 1981; Wallace and Gutzler 1983; Graham et al. 1995; Lau 1997; Hoerling and Ting 1994; Mantua et al. 1997), but there is continuing debate concerning the role of midlatitude SSTs on the

winter circulation over the North Pacific (Trenberth and Hurrell 1994; Latif and Barnett 1994; Blade 1997; Zhang et al. 1997; Peng et al. 1997). Whatever the driving mechanisms, variability in the time-averaged winter circulation has important effects on the environment and society through changes in precipitation, temperature, hydrologic and glaciological processes (Cayan and Peterson 1989; Dettinger and Cayan 1995; Bitz and Battisti 1999), upper-ocean characteristics (Miller et al. 1994; Deser et al. 1996; Overland et al. 1999), fisheries and marine ecosystems (Venrick et al. 1987; Beamish and Bouillon 1993; Polovina et al. 1995; Roemmich and McGowan 1995; Mantua et al. 1997), wave climate, and coastal processes (Seymour 1996; Ruggiero et al. 1997; Inman and Jenkins 1997; Allen and Komar 2000).

Although the majority of analyses of winter climate variability over the North Pacific concern seasonal to multiyear averages, it is important to recognize that variability at these timescales is intimately related to the transient fluctuations associated with individual midlatitude wave cyclones and migratory high pressure systems. Midlatitude cyclones are important from many perspectives. Among these are their dynamical roles in defining and maintaining the character of lower-frequency variability in the midlatitude circu-

*Scripps Institution of Oceanography, University of California, San Diego, La Jolla, California.

⁺Hydrologic Research Center, San Diego, California.

[#]NOAA Climate Diagnostics Center, Boulder, Colorado.

Corresponding author address: Dr. N. Graham, HRC, 12780 High Bluff Dr., San Diego, CA 92130.

E-mail: ngraham@ucsd.edu

In final form 16 January 2001.

©2001 American Meteorological Society

lation (e.g., Holopainen 1983; Held et al. 1989; Ting and Held 1990; Trenberth and Hurrell 1994) and their contributions to the transport of heat and moisture from the subtropics to higher latitudes and to the air-sea exchanges of heat and momentum (Peixoto and Oort 1992; Trenberth and Hurrell 1994; Hurrell and van Loon 1997). Further, intense cyclones and associated episodes of strong winds, high waves, and heavy precipitation are important in transmitting the effects of low-frequency climate variability to the environment and society.

In this paper, we describe evidence for changes in winter cyclone climatology over the North Pacific as seen in cyclone track statistics derived from the National Centers for Environmental Prediction–National Center for Atmospheric Research (NCEP–NCAR) reanalysis dataset covering 1948–98. In situ data from ocean station vessels, radiosonde reports, data buoys, and volunteer observing ships are used to corroborate the results. The paper is organized as follows. Data and methods are described in section 2, reanalysis results and comparisons with in situ data are presented in section 3, and section 4 gives a summary and discussion.

2. Data and methods

a. Cyclone analysis

Cyclone statistics were developed using sea level pressure (SLP) data from the reanalysis project conducted by the NCEP, NCAR, and other institutions and individual researchers (Kalnay et al. 1996). The 6-hourly SLP data were obtained from the National Oceanic and Atmospheric Administration's (NOAA) Climate Diagnostics Center on a $2.5^\circ \times 2.5^\circ$ latitude–longitude grid. An automated procedure was developed to identify and track individual cyclones (or “lows”) defined by local minima in SLP. A low was determined to occupy a grid point if that point had (a) the lowest surface pressure of the nearest three grid points in all directions (defining a region approximately $1100 \text{ km} \times 1500 \text{ km}$), and (b) a central pressure of less than 1000 hPa. These features were then tracked in time, requiring that an individual low move no faster than 100 km h^{-1} . A variety of statistics were recorded along each track, including central pressure and maximum geostrophic winds in the vicinity of the low. Because strong eddies are not always associated with closed surface lows (Sinclair and Watterson 1999), a variant of this procedure defined a “cyclone”

as a local maximum in relative vorticity, in this case requiring a central value of at least $5 \times 10^{-5} \text{ s}^{-1}$. In all cases, results are reported only for cyclones that had lifetimes of at least 24 h. The domain over which cyclones were tracked covered $30^\circ\text{--}50^\circ\text{N}$ and $150^\circ\text{E}\text{--}130^\circ\text{W}$ and the analysis covered the months of December–March for 1948/49 to 1997/98.

b. Other atmospheric data

Other NCEP–NCAR reanalysis datasets used in this analysis include monthly mean 850- and 200-hPa winds on the 2.5° grid, and 6-hourly near-surface (10 m) winds on a Gaussian grid with approximately 1.9° latitude–longitude spacing.

Data from the Comprehensive Ocean–Atmosphere Data Set (COADS; Woodruff et al. 1987) are also used. These include monthly mean and first sextile SLP and monthly mean surface winds for 1950–96. Related analyses use SLP and surface wind data from Ocean Station Vessels (OSVs, “weather ships”) 4YP (50°N , 145°W ; C7P in later years) and 4YN (30°N , 140°W). The portions of these records used cover December–March 1949–80 and 1948–72, respectively, at a nominal 3-hourly temporal resolution.

Other data used include wind (850 and 200 hPa) and SLP from Midway Island (28°N , 177°W) radiosonde observations. The portion of the record used here covers 1948–90, during which there were nominally two to four observations per day.

c. Sea surface temperature

The sea surface temperature data are those described by Smith et al. (1996). These monthly average data are on a $2^\circ \times 2^\circ$ latitude–longitude grid and cover the period from 1950 to the present.

d. Atmospheric model data

Upper-level (200 hPa) wind data are shown from simulations with an atmospheric general circulation model (AGCM). These data come from eight simulations with the Max Planck Institute for Meteorology ECHAM3 AGCM driven with observed global SSTs [those described by Smith et al. (1996)] over 1950–97. These simulations were driven by SST changes alone; there was no assimilation of observed atmospheric data and no changes in greenhouse gas concentrations. For these simulations, the ECHAM3 model was configured with 19 levels in the vertical and triangular-42 spectral truncation that gives a horizontal spacing of approximately 2.8° latitude and longitude. The ECHAM3 model is described fully in DKRZ

(1992); model characteristics and results of simulations may be found in Bengtsson et al. (1993).

e. Observed and hindcast wave data

We present measured and hindcast extreme significant wave heights (H_s ; a statistical parameter approximating the average of the highest one-third of the waves) from NOAA buoys 46011 (34.9°N, 120.9°W), 46006 (40.9°N, 137.5°W), and 51001 (23.4°N, 162.3°W). The measured data cover the late 1970s and early 1980s to the present, with some gaps, and were obtained from the NOAA National Data Buoy Center.

The ocean wave hindcast data come from a 50-yr simulation conducted by Pacific Weather Analysis, Inc. using the Wavewatch III model (Tolman 1999). The model was configured at a spacing of 1.5° latitude and 2° longitude using the 6-hourly reanalysis 10-m winds as forcing. Model output was obtained at 3-h intervals. Comparisons of the hindcast results with NOAA buoy wave data show very good agreement with respect to both specific events and interannual variability (correlations between 3-hourly measured and hindcast H_s are typically on the order of 0.85–0.90 for sites in the northeast Pacific). Details of the hindcast and results are described in Graham et al. (2001, manuscript in preparation). The model data used here are from the grid points closest to NOAA buoys 46011 (35°N, 120°W), 46006 (41°N, 138°W), and 51001 (23°N, 162°W). Also shown are the gridded trends in hindcast December–March 99th percentile wave height.

f. Statistical methods

The trends reported in our results are simple least squares linear fits to unsmoothed data (except in the case of the windowed data; see below). Trend significance levels were evaluated using *t*-tests with $n - 2$ degrees of freedom (where n is the length of the time series), a choice justified by the typical year-to-year autocorrelations of approximately 0.2–0.3. For the windowed samples (Figs. 2b–e; where the window width was approximately 10% of the sample size), n was set to 10, giving 8 degrees of freedom. Because estimates of linear trends are sensitive to minor changes in the data, and because the choice of the number of degrees of freedom is somewhat arbitrary in the presence of low-frequency variability, the trends and significance levels reported here should be interpreted as indicators rather than as specific values. All statistics concerning trends and their significance levels for individual time series are reported in Table 1.

Some of the analyses deal with 2–6-day root-mean-square (rms) SLP variability. For the gridded reanalysis data (Figs. 5a,b), these were calculated using an FFT and the filtering was done in frequency space using a 5% triangular taper outside the 2–6-day frequency window. Because there are gaps in the observational data from 4YN and Midway Island, band-passed SLP variability for both the in situ and reanalysis data from these locations was calculated using the Lomb–Scargle method (Lomb 1976; Scargle 1982; Press and Rybicki 1989; Press et al. 1992), which was designed for irregularly spaced data. Tests showed that the technique worked well as long as the gaps were not large, so results from years with more than 15% of the data missing are not shown.

3. Results

a. Climatology of North Pacific winter cyclones

To provide some background for the discussions that follow, this section provides a brief overview of the general climatology, or description of long-term means and interannual variation, of winter North Pacific wave cyclones. A typical North Pacific cyclone forms as a wave on the polar front, strengthens, matures, and decays over a period of several days, all while traveling several thousand kilometers. During this time, central pressures may fall 20–30 hPa (or more) and then rise again. Individual tracks vary considerably, but most intense lows in the North Pacific form west of the date line between 30° and 40°N, tracking first to the east and then curving toward the north as they mature and decay [e.g., Anderson and Gyakum (1989) and references therein]. Tracks and formation regions do show considerable interannual variability (e.g., Anderson and Gyakum 1989), and these changes have marked effects on the marine climate (e.g., Seymour et al. 1984; Strange et al. 1989; Inman and Jenkins 1997; Allen and Komar 2000). Figure 1 shows the long-term mean cyclone density as calculated from our results (note that like most cyclone statistics, reported density is sensitive to the counting criteria and tracking algorithm used). As can be seen, densities are highest [$> 9 (10^5 \text{ km}^2)^{-1}$ per season⁻¹] in the extreme northwestern North Pacific where many cyclones slowly decay, and lowest [$< 1 (10^5 \text{ km}^2)^{-1}$ per season⁻¹] in the southeastern part of the domain, reflecting the typical northeasterly cyclone tracks and the presence of the northeast Pacific subtropical anticyclone.

TABLE 1. Summary statistics for analyses of cyclone-related statistics (frequency, minimum central pressure, winds, and vorticity). Note: corr., anomaly correlation between data and linear trend; slope, linear trend; rmse, root-mean-square error of trend; $t = t$ statistic for trend; sig. = t -test significance (%); NS = t -test significance less than 85%; df, degrees of freedom. Regions: 1, 30°–40°N, 155°E–180°; 2, 30°–40°N, 180°–155°W; 3, 30°–40°N, 155°–130°W; 4, 40°–50°N, 155°E–180°; 5, 40°–50°N, 180°–155°W; 6, 40°–50°N, 155°–130°W.

(a) Cyclone frequency (df = 48; see Fig. 2a). Note: SLP thresh. is minimum central pressure threshold used (see text); slope is number of cyclones with MCP below threshold per year.

Region	N/SLP Tresh.	Corr.	Slope	Rmse	T	Sig.
1	289 / 980	0.50	0.083	0.021	3.95	>99.9
2	194 / 980	0.28	0.068	0.033	2.02	>95
3	107 / 986	0.37	0.053	0.020	2.72	>99
4	512 / 972	0.51	0.097	0.023	4.14	>99.9
5	428 / 972	0.51	0.159	0.039	4.06	>99.9
6	296 / 976	0.38	0.123	0.044	2.81	>99
All North Pacific	1128 / 975	0.48	0.21	0.056	3.76	> 99.9

(b) Minimum central pressure (df = 8; see Fig. 2b); slope = hPa yr⁻¹.

Region	N	Corr.	Slope	Rmse	T	Sig.
1	781	-0.49	-0.088	0.006	-15.60	>99.9
2	526	-0.19	-0.046	0.010	-4.54	>99
3	290	-0.01	-0.005	0.023	-0.22	NS
4	1380	-0.73	-0.098	0.002	-39.76	>99.9
5	1153	-0.62	-0.109	0.004	-27.05	>99.9
6	800	-0.19	-0.033	0.006	-5.51	>99.9
All North Pacific	2530	-0.67	-0.097	0.001	-45.29	>99.9

(c) Maximum windspeed (df = 8; see Fig. 2d); slope = m s⁻¹ yr⁻¹.

Region	N	Corr.	Slope	Rmse	T	Sig.
1	781	0.38	0.055	0.005	11.6	>99.9
2	526	0.48	0.089	0.007	12.6	>99.9
3	290	0.27	0.062	0.013	4.8	>99.9
4	1380	0.67	0.075	0.002	33.3	>99.9
5	1153	0.76	0.099	0.002	39.6	>99.9
6	800	-0.28	-0.034	0.004	-8.2	>99.9
All North Pacific	2530	0.72	0.075	0.001	52.4	>99.9

(d) Maximum zonal wind speed (df = 8; see Fig. 2e); slope = m s⁻¹ yr⁻¹.

Region	N	Corr.	Slope	Rmse	T	Sig.
1	781	0.63	0.086	0.003	22.4	>99.9
2	526	0.08	0.013	0.007	1.9	>90
3	290	0.16	0.037	0.014	2.7	>95
4	1380	0.71	0.082	0.002	37.8	>99.9
5	1153	0.62	0.073	0.003	26.8	>99.9
6	800	0.15	0.021	0.005	4.1	>99
All North Pacific	2530	0.76	0.065	0.001	58.7	>99.9

TABLE 1. (continued.)

(e) Vorticity center frequency (df = 48). Note: vort. thresh. is maximum vorticity threshold used ($\times 10^{-5} \text{ s}^{-1}$; see text); slope is number of cyclones with maximum vorticity > threshold per year.

Region	N/Vort. thresh.	Corr.	Slope	Rmse	T	Sig.
1	673 / 14.4	0.46	0.083	0.021	3.95	>99.9
2	597 / 13.1	0.29	0.068	0.033	2.02	>95
3	471 / 12.7	0.30	0.053	0.020	2.72	>99
4	868 / 16.3	0.22	0.097	0.023	4.14	>99.9
5	858 / 14.7	0.36	0.159	0.039	4.06	>99.9
6	707 / 13.8	0.27	0.123	0.044	2.81	>99
All North Pacific	1789 / 14.5	0.51	0.34	0.083	4.09	>99.9

(f) Maximum central vorticity (for vorticity center tracks; df = 8; see Fig. 2c); slope = $10^{-5} \text{ s}^{-1} \text{ yr}^{-1}$.

Region	N	Corr.	Slope	Rmse	T	Sig.
1	1818	0.74	0.065	0.001	45.6	>99.9
2	1613	0.58	0.039	0.001	28.9	>99.9
3	1272	0.36	0.018	0.001	13.9	>99.9
4	2346	0.75	0.056	0.001	54.8	>99.9
5	2318	0.72	0.049	0.001	49.4	>99.9
6	1911	-0.26	-0.011	0.001	-11.6	>99.9
All North Pacific	6141	0.76	0.037	0.0004	90.5	>99.9

(g) Maximum wind speed for vorticity centers (df = 8); slope = $\text{m s}^{-1} \text{ yr}^{-1}$.

Region	N	Corr.	Slope	Rmse	T	Sig.
1	1818	0.70	0.070	0.002	41.8	>99.9
2	1613	0.58	0.085	0.003	28.9	>99.9
3	1272	0.40	0.035	0.002	15.5	>99.9
4	2346	0.76	0.012	0.002	56.9	>99.9
5	2318	0.85	0.110	0.001	76.2	>99.9
6	1911	0.29	0.022	0.002	13.2	>99.9
All North Pacific	6141	0.85	0.075	0.0006	127.1	>99.9

(h) Maximum zonal wind speed for vorticity centers (df = 8); slope = $\text{m s}^{-1} \text{ yr}^{-1}$.

Region	N	Corr.	Slope	Rmse	T	Sig.
1	1818	0.84	0.097	0.001	65.5	>99.9
2	1613	0.46	0.059	0.003	20.6	>99.9
3	1272	0.46	0.050	0.003	18.5	>99.9
4	2346	0.67	0.086	0.002	43.0	>99.9
5	2318	0.80	0.108	0.002	65.7	>99.9
6	1911	0.05	0.005	0.002	2.2	>90
All North Pacific	6141	0.74	0.070	0.008	87.2	>99.9

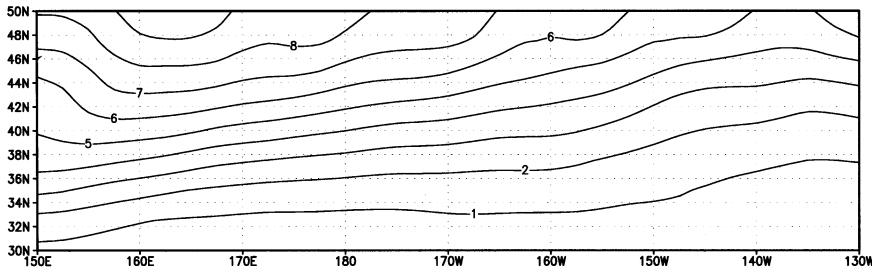


FIG. 1. Annual mean Dec–Mar cyclone density (10^5 km^{-2})⁻¹; smoothed with a nine-point spatial filter.

b. Cyclone statistics

The results from the cyclone tracking study reveal major changes in winter storm climate over the North Pacific during the past five decades not seen in previous studies. Figure 2a shows the frequency of deep North Pacific cyclones (number per winter season), defined as those with minimum alongtrack central pressure (MCP) less than 975 hPa (approximately the deepest one-third of the identified systems). For these

1128 systems, the record shows a clear upward trend in cyclone frequency superimposed upon substantial year-to-year variability. The linear trend of 0.21 cyclones per year is statistically significant above the 99.9% level (Table 1a) and represents an increase of 48% over the long-term mean. In agreement with other studies (Anderson and Gyakum 1989; Gyakum et al. 1989; Rogers 1990), the statistical association between cyclone activity and El Niño indices is modest: the anomaly correlation between the cyclone-count time series and the SST anomalies in the Niño-3.4 region (5°N–5°S, 120°–170°W) is 0.40 for 1950/51–1997/98. The record also shows a period with several years of high cyclone counts during the early 1980s, declining frequency during the late 1980s and early 1990s, and a return

(a)

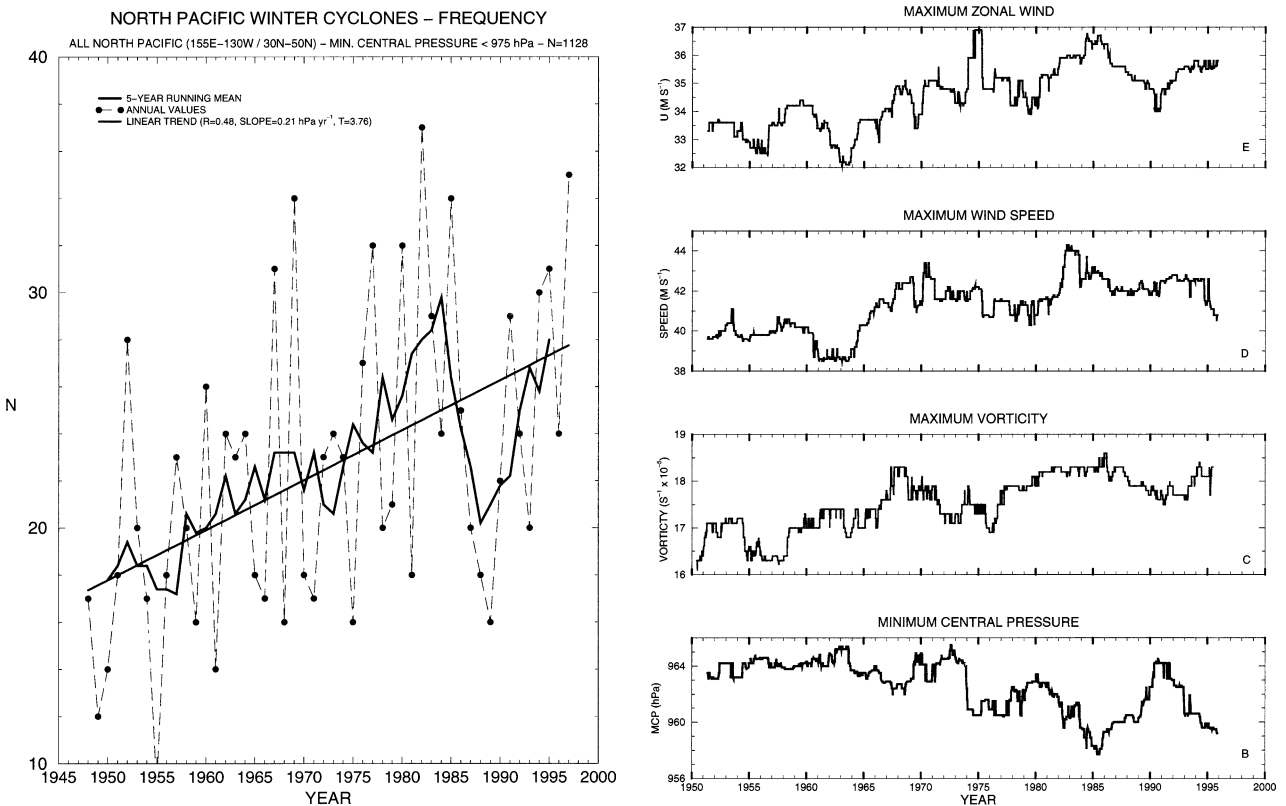


FIG. 2. (a) Time series of winter (Dec–Mar) counts of North Pacific cyclones with minimum central pressure less than 975 hPa. The curves show the raw data (dashed line with circles), the 5-yr running average (heavy solid line), and the linear trend. Time series of running 90th percentiles from North Pacific cyclones for a data window covering 10% of the total number of cyclones for (b) minimum central pressure, (c) maximum vorticity, (d) maximum wind speed, and (e) maximum zonal wind speed. Values in (b), (d), and (e) are calculated along the tracks of low pressure centers, (c) is calculated along the tracks of vorticity centers. See Table 1 for statistics.

toward higher values in the later years. No other clear suggestion of decadal-or-longer-timescale variability is readily apparent. When considered on a regional basis and using a spatially varying MCP cutoff (the lowest 33% MCP for each region), all areas show upward linear trends significant at the 95% level or higher, with the largest values in the regions north of 40°N and east of 180° (Table 1a).

To investigate changes in various indices of cyclone intensity, the following procedure was used.

Using MCP as an example, the MCPs of all identified lows for all years were listed sequentially. A sliding data window that was 10% of the full record length in width was passed over the record (i.e., if there were N entries in the list, the data window had a width of $N/10$). For each window position, the 10th percentile MCP value was recorded and dated as the median date in the data window. Note that, because the window width is defined in terms of number of cyclones (rather than units of time), the width of the data window in temporal units varies as the window is moved through the record.

The resulting record for MCP for the full North Pacific (Fig. 2b) shows a pronounced downward trend of approximately 4.9 hPa over 50 yr, with lower-frequency variability on timescales of 15–20 yr. The linear trend is significant above the 99.9% level and explains approximately 45% of the variance in the record (Table 1b). The records of cyclone frequency (Fig. 2a) and intensity (Fig. 2b) show some related features, with cyclones being deeper and more frequent in the mid-1960s, mid-1980s, and late 1990s and weaker and less frequent during the early 1970s and late 1980s/early 1990s.

To give an idea of the spatial distribution of changes in ex-

treme SLP, Fig. 3a shows trends in second percentile December–March SLP from the gridded 6-hourly re-analysis data. Negative trends dominate much of the North Pacific north of 35°N, with minima (reaching $-0.16 \text{ hPa yr}^{-1}$) near 50°N, 175°W and 45°N, 145°W and a lobe extending southeastward along the west coast of North America. Positive trends cover the western North Pacific south of 30°N and much of North America south of 55°N (and west of 110°W). Significance levels are above 95% over much of the

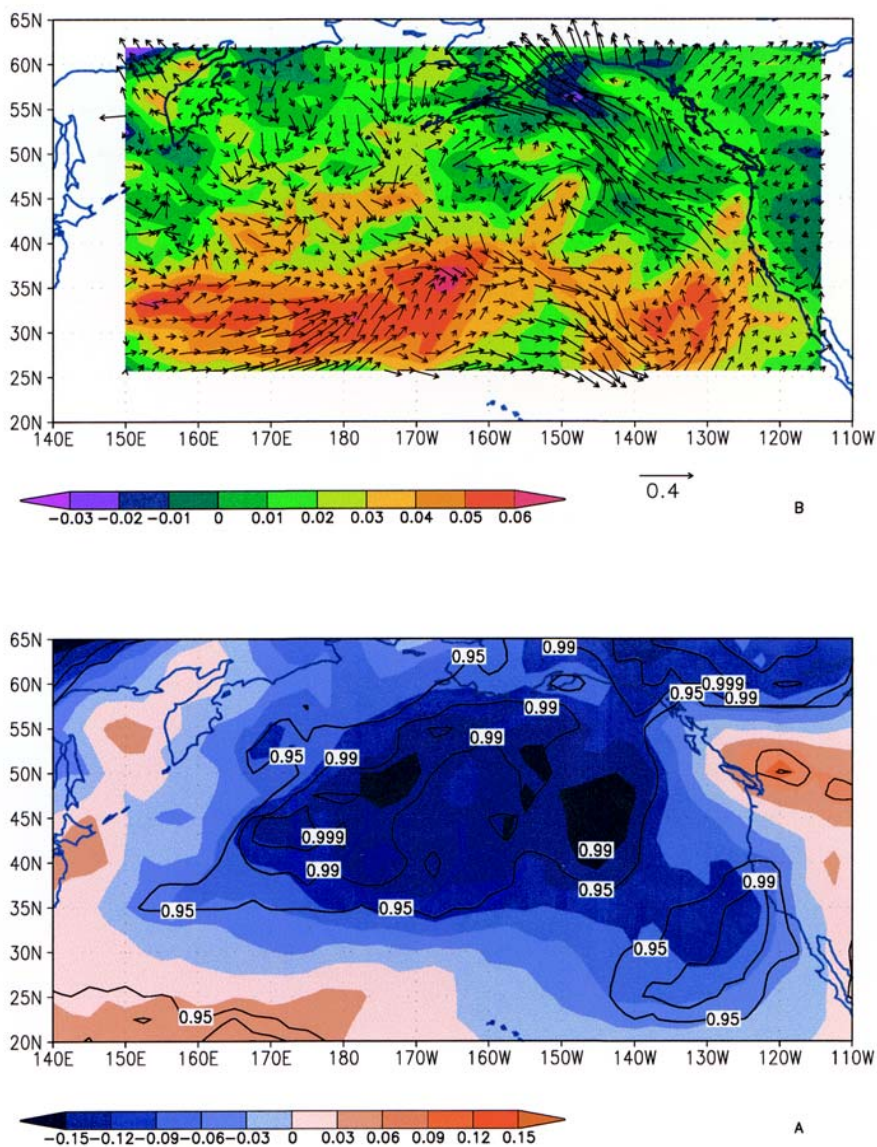


FIG. 3. (a) Linear trends in average Dec–Mar SLP less than or equal to annual second percentile (hPa yr^{-1}). T -test significance levels are shown by contours for 95%, 99%, and 99.9%. (b) Linear trends in annual Dec–Mar 99th percentile 10-m wind speed (contours give average of values above the 99th percentile). Vectors show trends in zonal and meridional components for cases in which the 99th percentile wind speed was exceeded ($\text{m s}^{-1} \text{ yr}^{-1}$). The 0.04 and 0.05 $\text{m s}^{-1} \text{ yr}^{-1}$ contours approximately correspond to the 95% and 99% significance levels, respectively.

central North Pacific poleward of 35°N and off the coast of California and northern Mexico. The corresponding map of trends in median SLP (not shown) shows a minimum near 45°N and 165°W [consistent with the results of other studies of decadal and interannual variability in seasonal means (e.g., Mantua et al. 1997; Trenberth and Hurrell 1994)]. Thus the largest negative trends in extreme low SLP are displaced to the west and east of the largest trends in median SLP.

The record of running 90th percentile maximum central relative vorticity for the full North Pacific (calculated for relative vorticity centers) is shown in Fig. 2c. The record is consistent with that for MCP (Fig. 2b) and shows an overall upward trend, with a maximum in the mid-1980s and a decline during the late 1980s and early 1990s, followed by a renewed upward trend. The linear trend is significant at greater than the 99.9% level (see Table 1f) and represents an increase of 11% in comparison with the long-term mean. On a regional basis, all of the records of maximum relative vorticity except that for the Gulf of Alaska (poleward of 40°N and east of 155°W) have positive trends that are significant above the 99.9% level (Table 1f). Some of the regional records show an intensification in the mid to late 1970s apparently associated with the well-documented changes in seasonal climate over the Pacific at that time (Nitta and Yamada 1989; Trenberth 1990; Graham 1994). In the Gulf of Alaska region, the trend is slightly negative and is significant above the 99.9% level.

These changes in cyclone climatology not surprisingly have been accompanied by trends in extreme wind speeds. The maximum geostrophic wind speed (MWS; note: 80% of the geostrophic wind speed was used as an approximation of the near-surface wind) for each cyclone was recorded as the maximum alongtrack geostrophic scalar wind speed in the 7 by 7 gridpoint box surrounding the cyclone center. The record of running 90th percentile MWS over the North Pacific (Fig. 2d) shows an upward trend from approximately 39 to 42 m s⁻¹ (approximately 8%), from 1955 through the early 1970s and a decline during the late 1970s, followed by a renewed upward trend. The linear trend explains approximately 50% of the total variance and is statistically significant above the 99.9% level (Table 1c). Regional trends in MWS range from -1.7 to 4.95 m s⁻¹ (all significant above the 99.9% level) per 50 yr, the sole negative value coming from the Gulf of Alaska region. Strong zonal winds are particularly important in establishing the extreme wave climatol-

ogy along much of the west coast of North America, and this record is shown in Fig. 1e. The record shows an upward tendency with a linear trend of approximately 3.25 m s⁻¹ over 50 yr, or approximately 10% of the long-term average value; this trend is significant above the 99.9% level. These trends in zonal wind speed are consistent with those calculated for the central North Pacific from seasonal mean SLP gradients using COADS ship reports (Diaz et al. 1994; Ward and Hoskins 1996). On a regional basis, the zonal wind trends (not shown) are upward [ranging from 0.086 to 0.013 (m s⁻¹ yr⁻¹)] and are significant above the 0.90 level in all regions except the south-central one (30°–40°N and 180°–155°W; see Table 1d).

In addition to the statistics for maximum central vorticity for cyclones defined on the basis of vorticity, Table 1 also gives statistics for frequencies, maximum wind speed, and maximum zonal winds for these features. Probably because vorticity is defined by the wind field, the wind statistics (Tables 1g,h) for the vorticity centers tend to show somewhat larger trends and substantially higher significance levels than those defined on the basis of MCP alone. The frequency statistics (Table 1e) show positive trends in all regions that are significant above the 95% level and an overall trend equivalent to an increase of 17 systems in 50 yr, amounting to approximately 5% of the long-term mean.

Figure 3b depicts the spatial changes in extreme near-surface winds, showing trends in annual December–March 99th percentile wind speed (from the 6-hourly 1.8° gridded data) and in the average vector wind components for analyses when wind speed exceeded the 99th percentile. The dominant feature is the band extending across the Pacific between 25° and 40°N, where wind speeds have increased by 2–2.5 m s⁻¹ in 50 yr. These values correspond approximately to the 95% and 99% significance levels, respectively. North of 35°–40°N, trends in extreme wind speed are smaller and become negative in a few places, most notably the Gulf of Alaska (consistent with the results seen in Table 1c). The coincident vector wind trends show features consistent with the trends in extreme low SLP (Fig. 3a). South of 40°N, the region of increasing wind speeds is dominated by strengthening westerlies, with typical values of 5–10 m s⁻¹ in 50 yr. The suggestion of a northeast–southwest-trending “ridge” north of the Hawaiian Islands is also apparent. Farther north, the most striking feature in the vector wind field is the region of southeasterly trends in the northeast Pacific and

Gulf of Alaska. The fact that these large trends in vector wind (up to 20 m s^{-1} in 50 yr) are associated with near-zero trends in near-surface wind speeds implies substantial changes in the favored circulation regimes accompanying intense storms (consistent with extreme SLP rising to the east and falling to the west, as shown in Fig. 3a). As discussed later, these trends are supported by the data from OSV 4YP (see Fig. 7b and related discussion), which show the favored extreme wind direction backing from west-northwest to south-southwest between 1950 and 1980. These changes in the character of extreme winds may have contributed to the changes in regional physical and ecological characteristics observed in the northeast Pacific (Mantua et al. 1997; Overland et al. 1999; Venrick et al. 1987; Polovina et al. 1995; Roemmich and McGowan 1995).

It is of interest to consider the degree to which the upward trends in frequencies of deep cyclones (Fig. 2a) and downward trends in MCP (Fig. 2b) reflect (a) an increasing total number of cyclones, (b) a decrease in background SLP, or (c) an increase in the relative frequency of deep cyclones. As noted by Whitaker and Sardeshmukh (1998), such an analysis presents some difficulty in that it presupposes separable background and transient fields. Nevertheless, Sinclair and Watterson (1999) show that lower central pressures do not always indicate more intense circulation. Figure 4 shows long-term mean cumulative frequency distribution (CDF) of winter cyclones as a function of MCP over the tracking domain (30° – 50°N and 155°E – 130°W) and the linear trends for each bin. The trends are upward for all bins, are statistically significant above the 99% level for all but the lowest two bins, and account for increasingly larger fractions of the mean frequency (ranging from 27% to more than 100%) as MCP declines. Also shown are the CDFs at the beginning and end of the analysis period as calculated by, respectively, subtracting and adding one-half the change accounted for by the linear trend to the long-term mean for each bin. Change due only to a decrease in background SLP would result in a downward shift (to the right) of the CDF for the early period. In Fig. 4, the early-period CDF has been shifted right by about one bin (5 hPa), approximating the magnitude of the trend in MCP seen in Fig. 2b (this value is also in agreement with the spatial trends in SLP shown in Figs. 3a and 6b). It is clear that the distribution is a poor approximation of the CDF for the later period. An alternative idea is that the trend toward increasing numbers of deep cyclones seen in Fig. 2a results solely

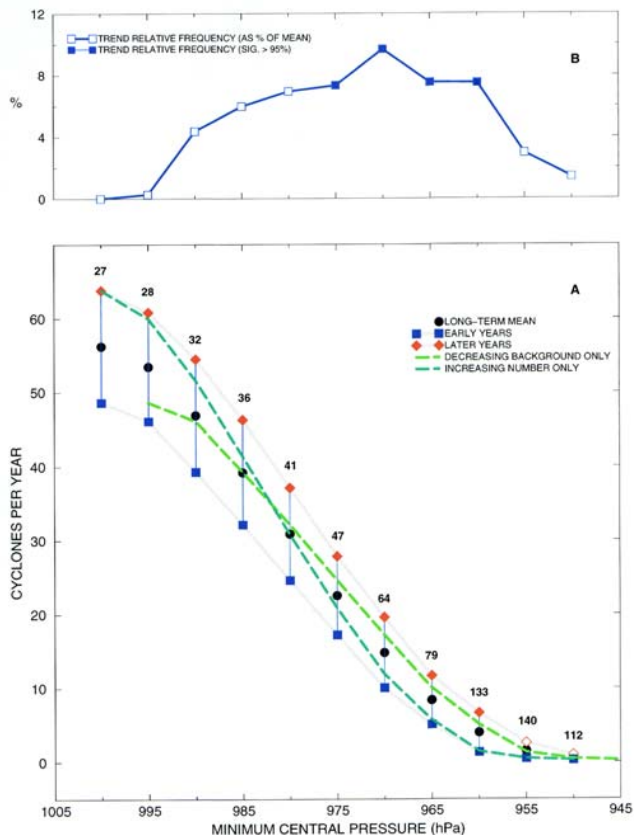


FIG. 4. (a) Long-term mean CDF of Dec–Mar minimum central pressure for North Pacific cyclones (black circles); lower gray curve with blue squares shows “early years” CDF, i.e., the long-term mean CDF less one-half of the linear trend in cumulative frequencies for each bin; gray curve with red squares shows the “later years” CDF, i.e., mean CDF plus one-half of the trend; blue bars connecting gray curves represent the trends for the CDF bins (per 50 years), filled red diamonds indicate that the trend is significant above the 99% level. Numbers indicate the fraction of the long-term mean represented by the trend. Green dashed curve shows the early years CDF (lower gray curve) shifted right by 5 hPa. Blue dashed curve shows the early years CDF multiplied so that the 1000-hPa value is equal to the value on the later years CDF (upper gray curve). (b) Trends in relative cyclone frequency expressed as fractions of long-term mean (filled squares indicate trends are significant above the 95% level).

from an increase in the total number of cyclones. In this case, the later-period CDF would be produced by stretching of the early-period CDF upward so that the leftmost points of the two CDFs (at 1000 hPa) are congruent. The resulting curve (Fig. 4) again does not agree well with the CDF for the later period. (A better match can be achieved by first shifting the early-period CDF 2.5 hPa to the right then stretching it upward to match the late-period curve.)

Another statistic related to the discussion above is relative cyclone frequency, defined here as the cumu-

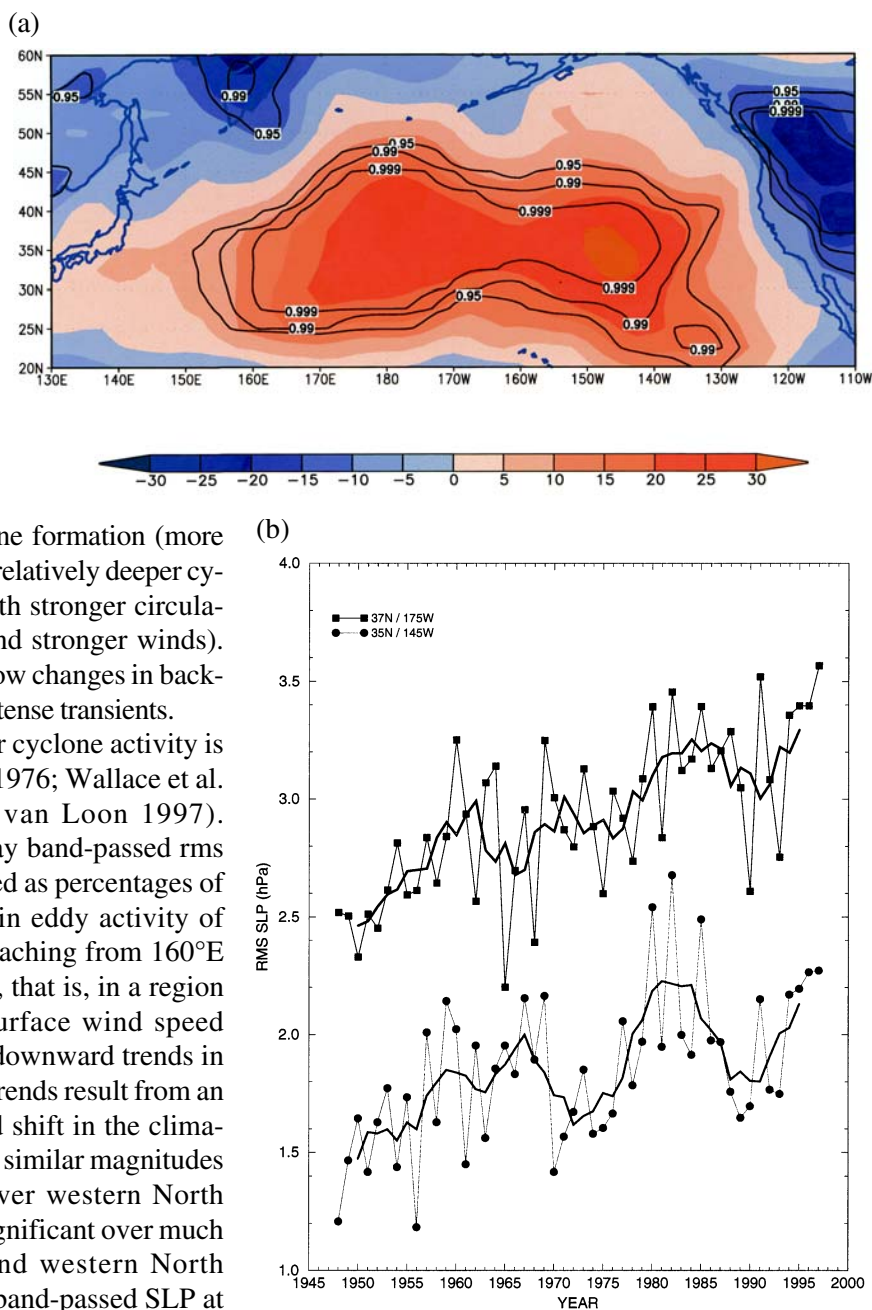
relative fraction of total cyclones with the MCP below a given threshold. Trends in relative cyclone frequency reflect changes in the shape of the CDF and are also shown in Fig. 4. These trends show the largest percentage increases to be in the range from approximately 985 to 960 hPa (the trends for the 960–975-hPa bins are significant above the 95% level). For lower MCPs, the trends are positive but much smaller. Thus the changes in reanalysis cyclone climatology are for relatively more frequent deep cyclones with MCP less than 975 hPa, though this effect does not apply to the rare cyclones with MCPs of 955 hPa or less.

Taken together, the results shown in Fig. 4 suggest that decreasing background SLP (itself closely related to the more vigorous transients) is partly responsible for the trends seen in Figs. 2a,b. At the same time, the stronger winds and vorticity seen in Figs. 2c–e demonstrate a trend toward stronger cyclone-associated circulations (on the order of 10%), something that would not occur if the only process at work was a decrease in background SLP. Thus, Figs. 2–4 also portray an environment increasingly favorable for cyclone formation (more cyclones), and for the evolution of relatively deeper cyclones (lower MCP; Fig. 4B), with stronger circulations (greater relative vorticity and stronger winds). Not addressed is the question of how changes in background SLP are related to more-intense transients.

Another useful index of winter cyclone activity is eddy variability (e.g., Blackmon 1976; Wallace et al. 1988; Lau 1988; Hurrell and van Loon 1997). Figure 5a shows trends in 2–6-day band-passed rms variability in winter SLP expressed as percentages of the long-term means. Increases in eddy activity of 10%–30% are found in a band reaching from 160°E to 135°W between 25° and 45°N, that is, in a region north of the maximum zonal surface wind speed changes and south of the largest downward trends in extreme low SLP. These upward trends result from an intensification and southeastward shift in the climatological mean field. Decreases of similar magnitudes in eddy activity are depicted over western North America. The trends are highly significant over much of the central North Pacific and western North America. The time series of rms band-passed SLP at

the two centers at 37°N, 175°W and 35°N, 145°W are shown in Fig. 5b. These records portray clear upward trends and pronounced low-frequency variability, repeating the pattern of relatively low values during the early 1970s and late 1980s to early 1990s, with higher values in the early 1980s and again toward the end of the record. The linear trends in these records (Table 2a) are significant above the 99.9% level.

What changes in the mean fields resulted in the trends seen in Figs. 5a,b? To address this question, Fig. 5c shows the average rms band-passed SLP for the first (1948/49–1972/73) and second (1973/74–



1997/98) 25 yr of the reanalysis data. It is apparent that the increasing band-passed variability reflects an equatorward shift of the contours (of up to about 3° of latitude) across the midlatitude North Pacific, suggesting a southward dip and eastward extension of the storm track. A similar figure (not shown) constructed using mean cyclone densities (as in Fig. 1) shows a qualitatively similar pattern, though the maximum increases are located 2°–4° north of their positions in Fig. 5c. Thus the increases in cyclone frequency and intensity discussed earlier did not result from a northward movement of the climatological storm track (where lows would tend to have lower central pressures), but rather from an intensification of the developing wave cyclones as they track eastward across the central North Pacific.

c. Comparisons with in situ data

Two key questions must be addressed when considering the reality of the trends seen in the reanalysis cyclone statistics for the North Pacific. First, are the trends artifacts of the observations? Second, are the trends artifacts of the reanalysis procedures? To minimize the potential for observational biases (the first question above) we use only datasets that satisfy the following criteria: (a) they are without suspected or established temporal bias; (b) these types of data have been widely used in climate analyses; and (c) they are

either from radiosonde stations, from OSVs, or have been subjected to strict quality-control procedures.

These datasets include volunteer observing ship (VOS) SLP data [quality-controlled data from COADS; see Woodruff et al. (1987)], wind and SLP reports from OSVs 4YN and 4YP, and radiosonde wind and SLP reports from Midway Island. Although individual VOS surface pressure reports are subject to uncertainties, aggregate VOS SLP reports are widely accepted as being without significant temporal bias (e.g., Ward 1992; Ward and Hoskins 1996). Further they form the basis of many analyses of low-frequency variability over the North Pacific and Atlantic (e.g., Trenberth 1990; Hurrell and van Loon 1997). OSV observing procedures were designed to produce reliable SLP and wind reports (e.g., Isemer 1994). Likewise, radiosonde SLP and wind reports (data from 850 and 200 hPa are used here) should not exhibit artificial temporal bias. Area-averaged VOS wind data from COADS are also shown in the comparisons below. In themselves, these data are not regarded as being as reliable as those described above (e.g., Cardone et al. 1990; Isemer 1994; Ward 1994). However, here the VOS wind record is shown to agree very closely with independent lower-tropospheric radiosonde wind data from Midway Island. A similar presentation of consistent evidence is made using reconstructed SST data [Smith et al. (1996); the original data are from VOS reports].

If the VOS (SLP), OSV, and radiosonde (SLP and wind) data discussed above are accepted as being without artificial secular bias, then the remaining source of spurious trends in the reanalysis results would be flaws in the reanalysis procedures (the second question above). If the reanalysis procedures produce spurious trends, then the reanalysis and in situ data should disagree. On the other hand, agreement between the reanalysis and reliable in situ data in terms of trends related to cyclone intensity would tend to support the reanalysis results, at least at the relevant locations. In the discussion below we compare a variety of in situ data with reanalysis results from nearby locations.

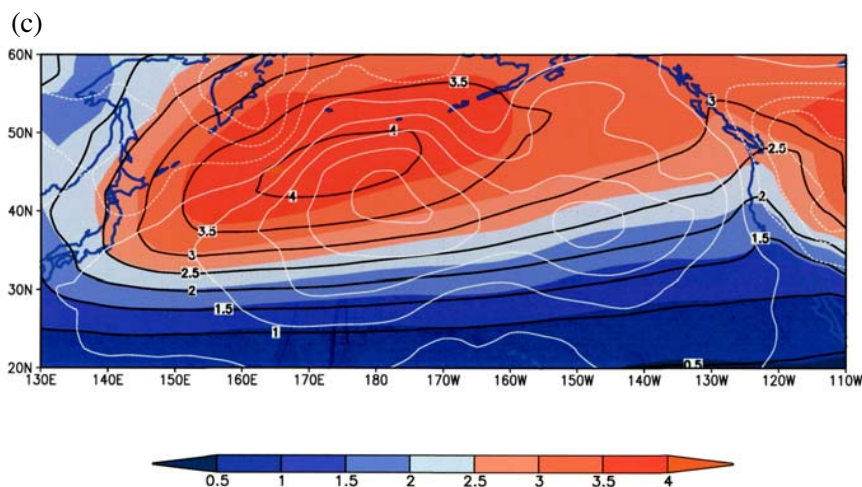


FIG. 5. (a) Linear trends in winter 2–6-day band-passed SLP as a percentage of the long-term annual mean (%). Contours show *t*-test significance levels. (b) Annual average 2–6-day band-passed SLP from 37°N, 175°W (upper curves) and from 35°N, 145°W (lower curves). Thin lines with symbols show raw data and heavy lines show 5-yr running averages. (c) Winter mean 2–6-day band-passed SLP for 1948/49 through 1972/73 (shaded contour map) and 1973/74 through 1997/98 (black contours; interval 0.5). White contours show the difference between the means [later years – earlier years; contour interval 0.1; highest contour (near 40°N, 180°) is 0.4].

TABLE 2. Summary statistics for analyses of time series from reanalysis gridded data, in situ observations, and wave hindcast results. Note: corr., anomaly correlation between data and linear trend; slope, linear trend; rmse, root-mean-square error of trend, T , t -statistic for trend; sig., t -test significance (%); NS, t -test significance less than 85%; df, degrees of freedom.

(a) The 2–6-day band-passed rms SLP (see Fig. 5b); slope = hPa yr ⁻¹ ; df = 48.						
Location	N	Corr.	Slope	Rmse	T	Sig.
37°N, 175°W	50	0.68	0.016	0.002	6.5	>99.9
35°N, 145°W	50	0.53	0.012	0.003	4.3	>99.9

(b) First sextile SLP (35°–45°N, 180°–140°W) 1949/50–1996/97 (df = 45; see Fig. 6c); slope = hPa yr ⁻¹ ; RA = reanalysis.						
Data	N	Corr.	Slope	Rmse	T	Sig.
COADS	47	-0.46	-0.146	0.042	-3.44	>99.9
RA	47	-0.38	-0.128	0.046	-2.77	>99

(c) First sextile SLP; OSV 4YP (see Fig. 6d); slope = hPa yr ⁻¹ ; OBS = 4YP (1949/50–1980/81; N = 32; df = 30); CO = COADS (same as obs); RA1 = reanalysis (same as obs); RA2 = reanalysis (1948/49–1997/98; N = 50, df = 48).						
Data	N	Corr.	Slope	Rmse	T	Sig.
OBS	32	-0.32	-0.170	0.092	-1.84	>90
CO	32	-0.30	-0.150	0.100	-1.73	>90
RA1	32	-0.27	-0.124	0.072	-1.51	>85
RA2	50	-0.35	-0.129	0.049	-2.65	>98

(d) First sextile SLP; OSV 4YN (see Fig. 6e); slope = hPa yr ⁻¹ ; OBS = 4YN [1949/50–1972/73; N = 22 (1950/51, 1952/53 missing), df = 20]; CO = COADS (same as obs); RA = reanalysis (same as obs); RA1 = reanalysis (1948/49–1997/98; N = 50, df = 48).						
Data	N	Corr.	Slope	Rmse	T	Sig.
OBS	22	-0.20	-0.095	0.107	-0.884	NS
CO	22	-0.23	-0.115	0.112	-1.020	NS
RA1	22	-0.17	-0.073	0.100	-0.729	NS
RA2	50	-0.39	-0.082	0.018	-2.920	>99

(e) Second percentile SLP; OSV 4YP (see Fig. 7a); slope = hPa yr ⁻¹ ; OBS = radiosonde (1949/50–1972/73; N = 32 due to missing years, df = 30); RA1 = reanalysis (same as obs, df = 30); RA2 = full reanalysis (N = 50, df = 48).						
Data	N	Corr.	Slope	Rmse	T	Sig.
OBS	32	-0.16	-0.095	0.102	-0.93	NS
RA1	32	-0.21	-0.123	0.105	-1.17	NS
RA2	50	-0.34	-0.145	0.058	-2.49	>98

(f) Second percentile SLP; OSV 4YN (see Fig. 7b); slope = hPa yr ⁻¹ ; OBS = 4YN [1948/49–1973/74; N = 23 (1950/51, 1951/52, 1952/53 missing), df = 21]; RA1 = reanalysis (same as obs, df = 21), RA2 = full reanalysis (N = 50, df = 48).						
Data	N	Corr.	Slope	Rmse	T	Sig.
OBS	22	-0.15	-0.083	0.122	-0.68	NS
RA1	22	-0.12	-0.074	0.136	-0.54	NS
RA2	50	-0.28	-0.090	0.045	-2.00	>94

(g) The 2–6-day rms SLP variability, OSV 4YN (see Fig. 8a); slope = hPa yr ⁻¹ ; OBS = radiosonde (1948/49–1972/73; N = 22 due to dropped years, df = 20); RA1 = reanalysis (same as obs), df = 20); RA2 = full reanalysis (N = 50, df = 48).						
Data	N	Corr.	Slope	Rmse	T	Sig.
OBS	20	0.43	0.027	0.012	2.15	>95

TABLE 2. (Continued.)

RA1	20	0.40	0.023	0.012	1.93	>98
RA2	50	0.35	0.010	0.004	2.60	>98

(h) The 2–6-day rms SLP variability; Midway Island (see Fig. 8b); slope = hPa yr⁻¹; OBS = radiosonde (1949/50–1989/90; $N = 32$ due to dropped years, $df = 30$); RA1 = reanalysis (same as obs); RA2 = full reanalysis ($N = 50$, $df = 48$).

Data	N	Corr.	Slope	Rmse	T	Sig.
OBS	32	0.28	0.007	0.004	1.59	>88
RA1	32	0.49	0.011	0.004	3.10	>99
RA2	50	0.54	0.011	0.002	4.40	>99.9

(i) The 95th percentile wind speed: OSV 4YN (see Fig. 9a); slope = ms⁻¹ yr⁻¹; OBS1 = 4YN [1948/49–1973/74; $N = 23$ (1950/51 and 1952/53 missing), $df = 21$]; OBS2 = 4YN [1948/59–1971/72; $N = 21$ (1950/51, 1951/52, 1952/53 missing, 1972/73, 1973/74 deleted), $df = 19$]; RA1 = reanalysis (same as OBS1, $df = 21$); RA2 = reanalysis (same as OBS2, $df = 19$); RA3 = reanalysis (1948/49–1997/98; $N = 50$, $df = 48$).

Data	N	Corr.	Slope	Rmse	T	Sig.
OBS1	23	0.56	0.210	0.068	3.08	>99
OBS2	21	0.41	0.127	0.065	1.93	>90
RA1	23	0.52	0.068	0.024	2.79	>98
RA2	21	0.47	0.066	0.029	2.31	>95
RA3	50	0.55	0.045	0.010	4.57	>99.9

(j) Reanalysis zonal winds and shear: 30°–35°N, 180°–155°W ($df = 48$; see Fig. 10a); slope = m s⁻¹ yr⁻¹.

Data	N	Corr.	Slope	Rmse	T	Sig.
200-hPa U	50	0.45	0.193	0.055	3.53	>99.9
U shear	50	0.44	0.109	0.032	3.38	>99
850-hPa U	50	0.43	0.086	0.026	3.27	>99

(k) Midway Island zonal winds and shear (1949/50–1989/90; $df = 39$; see Fig. 10a); slope = m s⁻¹ yr⁻¹.

Data	N	Corr.	Slope	Rmse	T	Sig.
200-hPa U	41	0.38	0.210	0.081	2.60	>98
U shear	41	0.32	0.146	0.069	2.12	>95
850-hPa U	41	0.27	0.064	0.037	1.74	>90

(l) COADS zonal surface winds: 30°–35°N, 180°–155°W; 1949–94 ($df = 44$; see Fig. 10a); slope = m s⁻¹ yr⁻¹.

Data	N	Corr.	Slope	Rmse	T	Sig.
Surface U	44	0.34	0.052	0.022	2.38	>95

(m) SST: 30°–35°N, 180°–155°W; 1949–97 ($df = 47$; see Fig. 10b); slope = C yr⁻¹.

Data	N	Corr.	Slope	Rmse	T	Sig.
SST	49	0.50	0.021	0.005	3.98	>99.9

(n) Hindcast 95th percentile significant wave heights ($df = 48$; see Figs. 11a–c); (see Fig. 12a for locations); slope = m yr⁻¹.

Data	N	Corr.	Slope	Rmse	T	Sig.
46011	50	0.49	0.025	0.006	4.00	>99.9
46006	50	0.36	0.021	0.008	2.67	>98
51001	50	0.39	0.014	0.048	2.95	>99

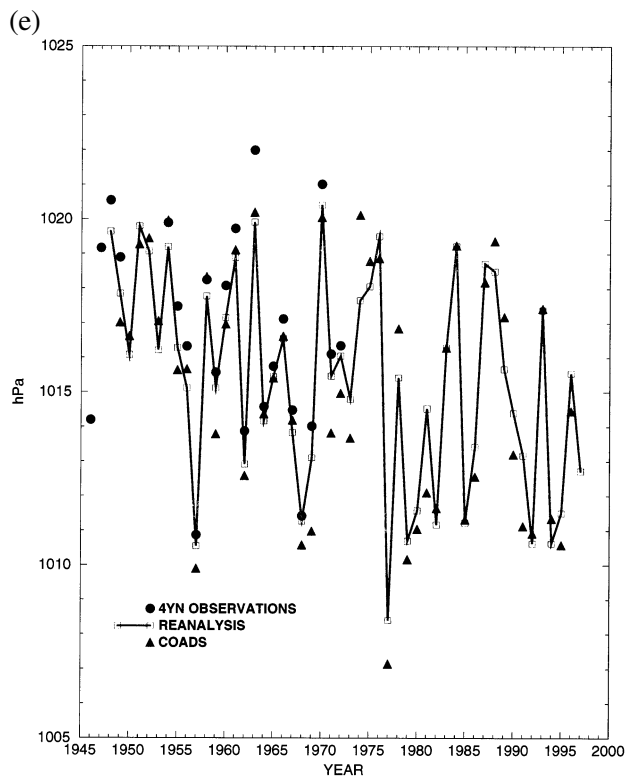
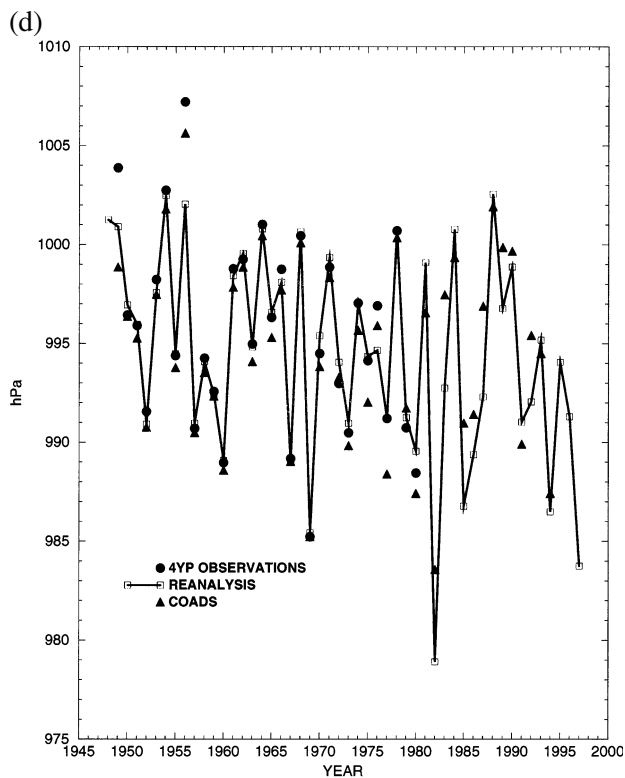
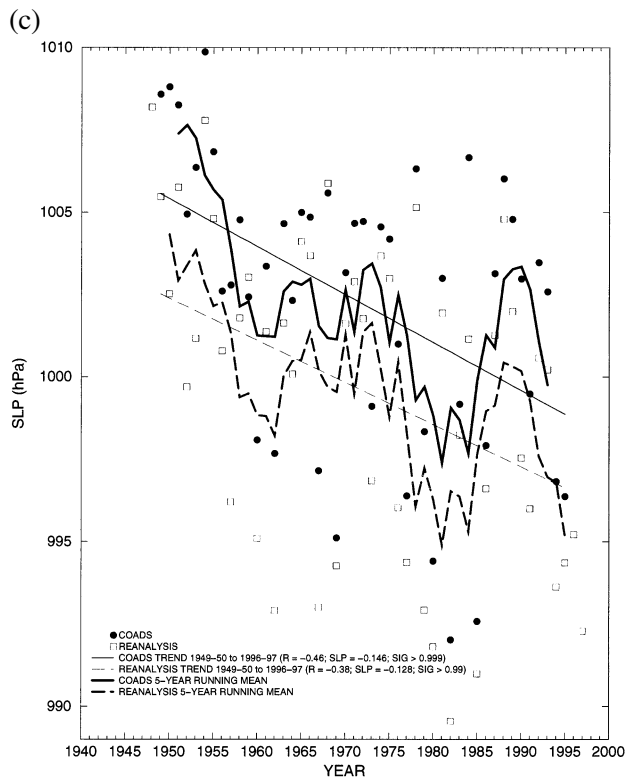
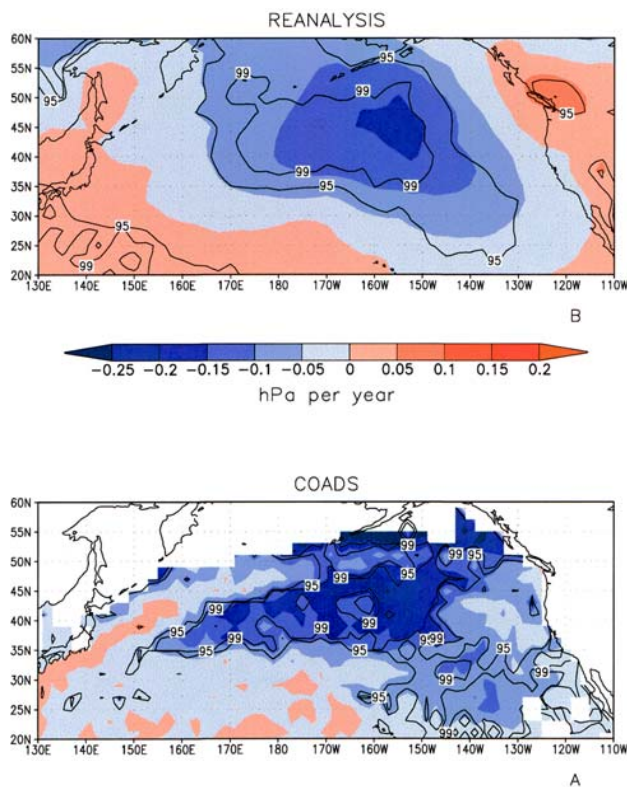


FIG. 6. (a) Linear trends (hPa yr^{-1}) and t -test significance levels for mean Dec–Mar first sextile SLP from COADS, 1950/51–1996/97. (b) As in (a), but for reanalysis SLP. (c) Time series of area-average first sextile SLP from COADS (solid curves) and reanalysis (dashed curves) over the region 35° – 40° N and 180° – 140° W; symbols show raw data, heavy curves are 5-yr running means, and straight lines are linear trends. (d) First sextile SLP from OSV 4YP, COADS, and reanalysis. (e) As in (d), but for OSV 4YN.

For low surface pressure, the relevant VOS product available from COADS is monthly first sextile SLP. [Although the first sextile values are not “extreme,” analyses of OSV reports (not shown) show that the records of winter mean first sextile and second percentile SLP are highly correlated.] The trends in average December–March first sextile SLP from COADS (Fig. 6a) show negative values covering much of the North Pacific poleward of 35°N and east of 160°E, with a secondary lobe extending southeastward into the subtropical eastern ocean. Over much of this region, the trends are highly significant (> 95%–99%) and range from -0.1 to -0.2 hPa yr⁻¹, with minimum values less than -0.25 hPa yr⁻¹ along 45°N between 180° and 150°W. The corresponding figure for the reanalysis data (Fig. 6b) also shows statistically significant negative trends covering much of the central and southeastern North Pacific. In the central North Pacific, the reanalysis trends are smaller than those from COADS and show near-zero trends rather than negative values in the eastern Gulf of Alaska. Comparisons of the datasets indicate that these differences appear to result from sharp decreases in the COADS values during the early 1950s that are more muted in the reanalysis results. The trend maps also differ in the western ocean, with the reanalysis result lacking the pronounced westward extension of negative trends between 35° and 45°N. Despite these differences, the two datasets agree in showing highly significant downward trends in December–March first sextile SLP over much of the eastern North Pacific poleward of 30°N.

The temporal agreement between the COADS and reanalysis first sextile SLP data is emphasized in Fig. 6c, which shows the annual December–March averages and 5-yr running mean first sextile SLP for the region 35°–40°N and 180°–140°W. The excellent agreement between the datasets is clear (the correlation between the unsmoothed time series is 0.93), as is the indication of a downward trend (-0.15 and -0.12 hPa yr⁻¹, respectively, significant at above the 99% level), with decadal-scale variability much like that seen in other records discussed earlier. Also apparent is the discrepancy between the COADS and re-

analysis records during the early 1950s referred to above.

Further corroborative comparisons can be made using the SLP reports from OSVs 4YP and 4YN. The time series for first sextile SLP from the OSVs, COADS, and reanalysis are shown in Figs. 6d and 6e. For 4YP (Fig. 6d), the datasets show excellent agreement, with a correlation of 0.97 and downward trends that are in good agreement (ranging from -0.12 hPa yr⁻¹ for the reanalysis to -0.17 hPa yr⁻¹ for 4YP; see Tables 2b,c). The reanalysis trend for the early part of the record and for the full record are nearly identical (-0.124 vs -0.129 hPa yr⁻¹). For 4YN (Fig. 6e), the agreement between the datasets is also good, with a correlation of 0.96 and trends ranging from -0.073 (reanalysis) to -0.115 hPa yr⁻¹ (COADS) for those years with relatively complete records from 4YN between 1949 and 1971. Again, the reanalysis trend over the full record (-0.082 hPa yr⁻¹) is similar to that for the

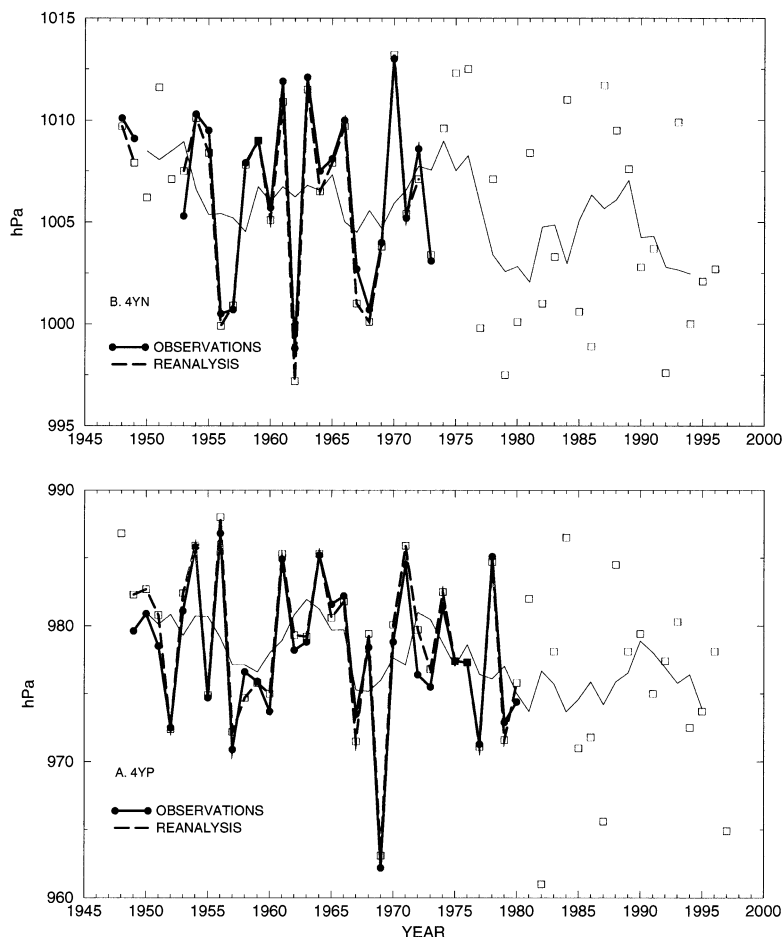


FIG. 7. Second percentile Dec–Mar SLP from reanalysis and (a) OSV 4YP and (b) OSV 4YN. Blue squares show annual reanalysis values; thin blue lines are 5-yr running means for reanalysis; heavy solid lines with circles are OSV observations; heavy dashed lines are reanalysis data.

earlier portion of the record and is significant above the 99% level.

Comparisons of observed and reanalysis extreme (second percentile) SLP at 4YP and 4YN are shown in Fig. 7. Again the datasets agree very well during the periods of overlap, with correlations of 0.98 and 0.99, respectively. At both sites, but particularly at 4YP, the observational record supports the presence of decadal variability seen in the low-passed reanalysis record. Both sites show similar downward trends in the shorter early records and in the full reanalysis record (see Tables 2d,e), though the high degree of interannual variability and short records yield trends for the observational period that are nonsignificant.

To corroborate trends in 6–10-day rms SLP variability seen in the reanalysis data (Figs. 5a,b), the 4YN and Midway Island radiosonde SLP reports were used. Their location on the southern flank of the region

where the reanalysis data show large and highly significant upward trends in RMS SLP variability (see Fig. 5a) makes these stations relevant for this analysis. For 4YN (Fig. 8a), the in situ and reanalysis records agree well (the correlation between the two is 0.92; see Tables 2f,g for statistics). The records also show some of the decadal-scale variability apparent in other results. The upward trend for the full reanalysis record is apparent ($0.0096 \text{ hPa yr}^{-1}$, significant above the 90% level). For Midway Island (Fig. 8b) the reanalysis and observed datasets again agree well ($r = 0.91$), and each exhibits low-frequency variability superimposed on statistically significant upward trends (see Table 2g; note: the significance level of the Midway Island trend is just below the 90% level). As a further point of corroboration, a plot of RMS SLP prepared by M. Dettinger (2000, personal communication; not shown) for 35°N , 175°W using $5^\circ \times 5^\circ$ data (Trenberth and Paulino 1980) shows an upward trend and decadal features similar to those seen in Figs. 5b and 8b. [The in situ and reanalysis 6–10-day RMS SLP records from 4YP (not shown) are also similar ($r = 0.92$), with neither showing significant trends.]

For comparisons of OSV and reanalysis wind data, Figure 9a shows the 95th percentile wind speed records for 4YN. For these data, there is relatively good agreement with regard to year-to-year fluctuations (the correlation is 0.81), although the OSV observations show higher values and more variability than the reanalysis data. The upward trends in datasets are clear (and statistically significant above the 90% level; see Table 2h), though the magnitude of the trend in the ship observations is nearly 2 times as large. [This difference in magnitude is largely due to the values in the last two years of the observed record; removing these years reduces the trend by 40%, but it remains larger than the reanalysis trend for the corresponding years (see Table 2h).] For the full time period, a relatively steady upward trend of $0.045 \text{ m s}^{-1} \text{ yr}^{-1}$ is apparent in the reanalysis data, significant at above the 99.9% level. [Consistent with Fig. 3a, the reanalysis 95th percentile wind speed record from 4YP (not shown) shows no

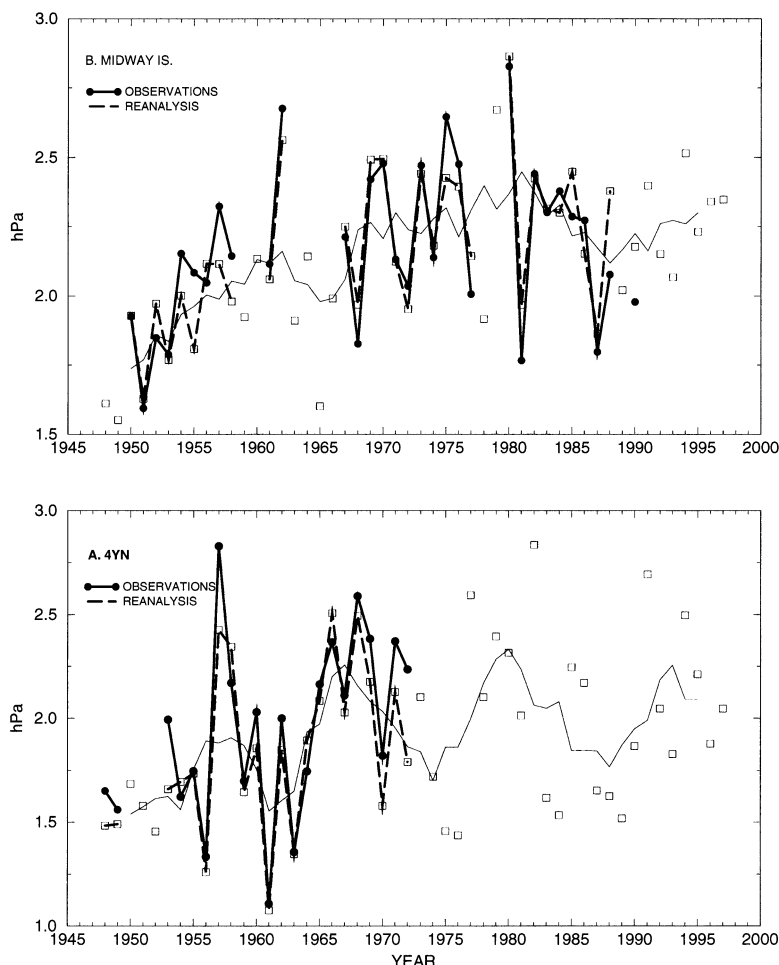


FIG. 8. Six-to-ten-day rms SLP variability from reanalysis and (a) OSV 4YN and (b) Midway Island. Blue squares show annual reanalysis values; thin blue lines are 5-yr running means; heavy solid lines with circles are OSV observations; heavy dashed lines are reanalysis data.

significant trend. However, for the 1949–80 period, the OSV observations show a considerable downward trend in 95th percentile wind speeds. Whether this observed trend is real or resulted from changes in instrumentation is not known.]

Figure 9b compares the observed and reanalysis records of vector-average wind direction for 4YP for cases when wind speed exceeded the 95th percentile for a given winter. During the 1949–80 period of overlap, there is good agreement between the two records, with both suggesting an irregular trend of backing from the west-northwest toward the west-southwest before 1970 and a major change at the end of the in situ record. The reanalysis data indicate a partial return toward the pattern of earlier years during the last portion of the record. Thus the observed data support the major trends in wind direction seen over the Gulf of Alaska in Fig. 3a. A corresponding analysis for 4YN (not shown) also shows good agreement between the observed and reanalysis wind direction records, with no major trends in preferred wind direction during periods of high winds.

Further useful comparisons can be made between the winds-aloft data from the Midway Island radiosonde record and the reanalysis data. As will be discussed later, this comparison is particularly important because upward trends in upper-level westerlies and resulting vertical wind shear over the midlatitude North Pacific are viewed as contributing to the intensification of North Pacific cyclones. Figure 10a shows the time series of 5-yr running mean observed winter-averaged zonal winds at 200 and 850 hPa (approximately 1.5 and 11.8 km above mean sea level, respectively) from Midway Island. The corresponding reanalysis data are for the region 30°–35°N and 180°–155°W in which the rms SLP trends are most significant (see Fig. 3a). For 200 hPa, the observed and reanalysis zonal wind records agree very well with respect to both decadal variability and the presence of substantial upward trends. The correlation between the unsmoothed datasets is 0.72, and the trends are 0.19 and 0.21 $\text{m s}^{-1} \text{yr}^{-1}$ for the reanalysis and observations, respectively, sig-

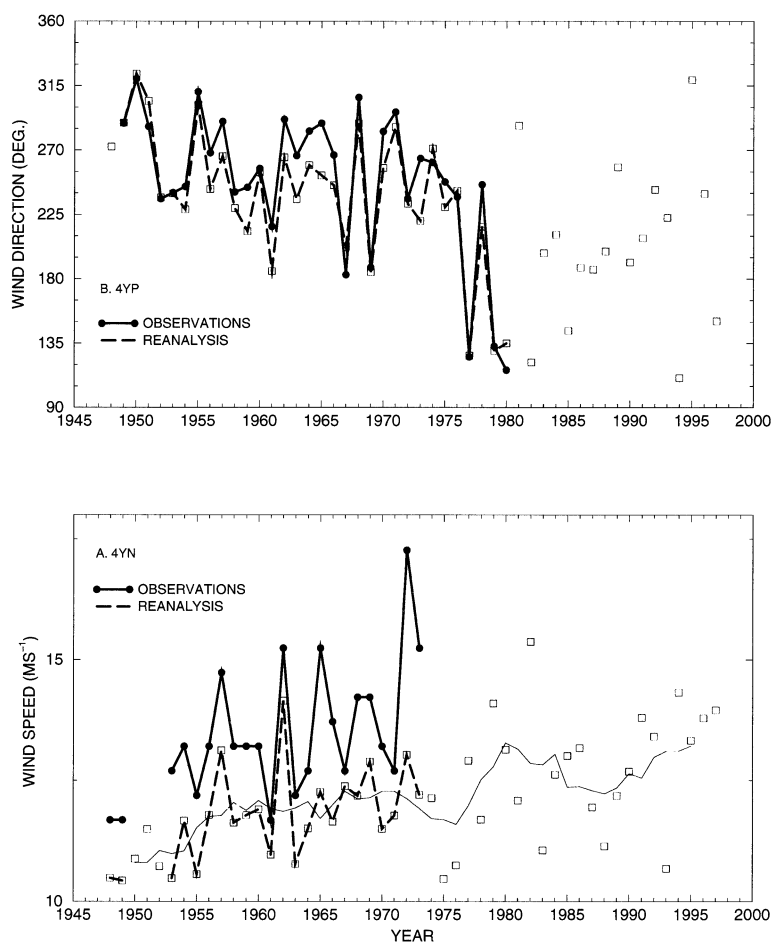


FIG. 9. (a) The 95th percentile wind speeds from OSV 4YN and reanalysis. (b) Vector average wind direction for cases in which wind speed exceeded 95th percentile for OSV 4YP and reanalysis. Blue squares show annual reanalysis values; thin blue lines are 5-yr running means; heavy solid lines with circles are OSV observations; heavy dashed lines are reanalysis data.

nificant above the 98% level (see Tables 2i,j). The 850-hPa zonal wind records also agree very well (the correlation of the unsmoothed datasets is 0.91) and again have statistically significant (>95%) and obvious upward trends. For the 850 hPa, the trends (0.064 and 0.086 for the observed and reanalysis data, respectively) would result in changes in zonal wind over the full record of 3–4 m s^{-1} , or 60%–80% of the mean values. The records of running average 200–850-hPa zonal wind shear not surprisingly also agree well (the correlation for the unsmoothed data is 0.55), and again both datasets have statistically significant trends (>95%) that amount to 20%–25% of the respective mean values. Note that each of the upper-level wind records in Fig. 10a shows some agreement with the records of rms SLP activity depicted in Fig. 5b, a point that will be discussed below.

Further verification of the reality of the wind changes (and by extension the changes in reanalysis cyclone climatology) come from COADS area-averaged zonal surface winds (Fig. 10a; again for 30°–35°N and 180°–155°W). There is close agreement between the record of 850-hPa zonal winds from Mid-

way and the area-averaged COADS zonal winds [the correlation is 0.84 for the overlapping portions (1949–89) of the unsmoothed datasets] with regard to both interdecadal variability and the presence of significant upward trends. The trend of the COADS data for 1949–94 is $0.052 \text{ m s}^{-1} \text{ yr}^{-1}$, significant above the 95% level.

It is important to note that the COADS surface wind and Midway Island radiosonde datasets are completely independent; their agreement provides strong support for the reality of the very similar changes seen in the reanalysis results. A corresponding argument can be made using SST data from the same region (30°–35°N and 180°–155°W). As can be seen in Fig. 10b, these data show a decreasing trend consistent with increasing heat fluxes and mixing associated with increasing surface winds [e.g., Cayan et al. (1993); Miller et al. (1994); Deser et al. (1996); Ward and Hoskins (1996); the SST trend is $-0.02^\circ\text{C yr}^{-1}$, significant above the 99.9% level]. Further, the decadal-scale variability in the SST data is similar to that seen in the wind data shown in Fig. 10a (e.g., the correlations between the SST data and the unsmoothed Midway 850-hPa zonal winds and COADS surface zonal winds are 0.47 and 0.66, respectively, both significant at above the 99% level).

A final in situ comparison relates to the accuracy of the latter part of the reanalysis wind record and to the impacts the changes in reanalysis surface winds would have on ocean wave climate. Figure 11 shows annual December–March 95th percentile H_s (see section 2e) for locations off the central California coast, in the open-ocean eastern Pacific, and northeast of Hawaii from buoy observations and from the wave

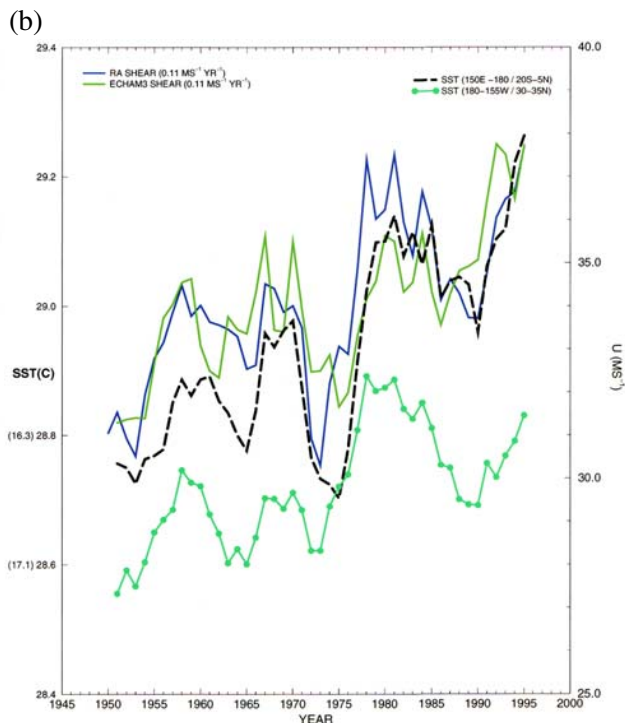
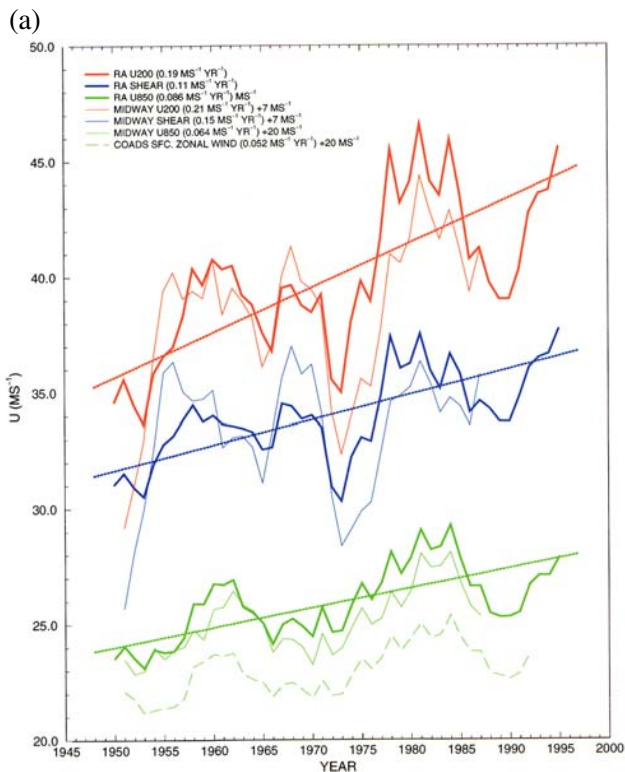


FIG. 10. (a) The 200- and 850-hPa zonal wind and zonal wind shear from reanalysis results (area average over 30°–35°N and 180°–155°W; heavy solid red, blue, and green lines) and from Midway Island radiosonde observations (thin solid red, blue, and green lines). Also shown are mean zonal surface winds from COADS (thin dashed green line). Linear reanalysis trends are shown as heavy dotted lines. Note that 7 m s^{-1} has been added to the Midway Island 20-hPa zonal winds and 200–850-hPa zonal wind shear, and 20 m s^{-1} has been added to the Midway Island 850-hPa and COADS surface zonal wind records. (b) The 200–850-hPa zonal wind shear from the reanalysis (heavy blue line, repeated from Fig. 8a) and from the ECHAM3 AGCM (heavy green line; area averaged over 20°–35°N and 180°–155°W); area-averaged SST from 30°–35°N and 180°–155°W (heavy turquoise line with circles; note that the scale for this curve is inverted—values are shown on abscissa in parentheses); area-averaged SST from 20°S–5°N, 150°E–180° (heavy dashed black line). All curves in (a) and (b) are for Dec–Mar and show 5-yr running means, except those of SST, which show the annual values.

model hindcast (NOAA buoys 46011, 46006, and 51001, respectively; see Fig. 12a for locations). For the period during which they overlap, the observed and hindcast records show a period of high extreme waves during the 1980s, a decline during the late 1980s and early 1990s, and a return toward higher waves toward the end of the record [Allen and Komar (2000) show similar decadal variability for buoy 46005 off the coast of Washington]. The similarities in the observed and hindcast wave records show that the reanalysis wind data (and the wave model) are sufficiently accurate to reproduce observed low-frequency variability in extreme-wave activity during the 1980s and 1990s. Prior to the onset of observations, the reconstructed records at the NOAA buoy locations exhibit substantial upward trends [the trends are significant at above the 98% level (see Table 2m)] that represent increases of approximately 35%–70% in terms of energy.

Spatially, the trends in hindcast extreme wave heights (99th

percentile H_s ; Fig. 11d) reflect the trends toward increasing extreme westerlies south of 40°N (Fig. 3b). These trends show increases of 1–2.5 m across much

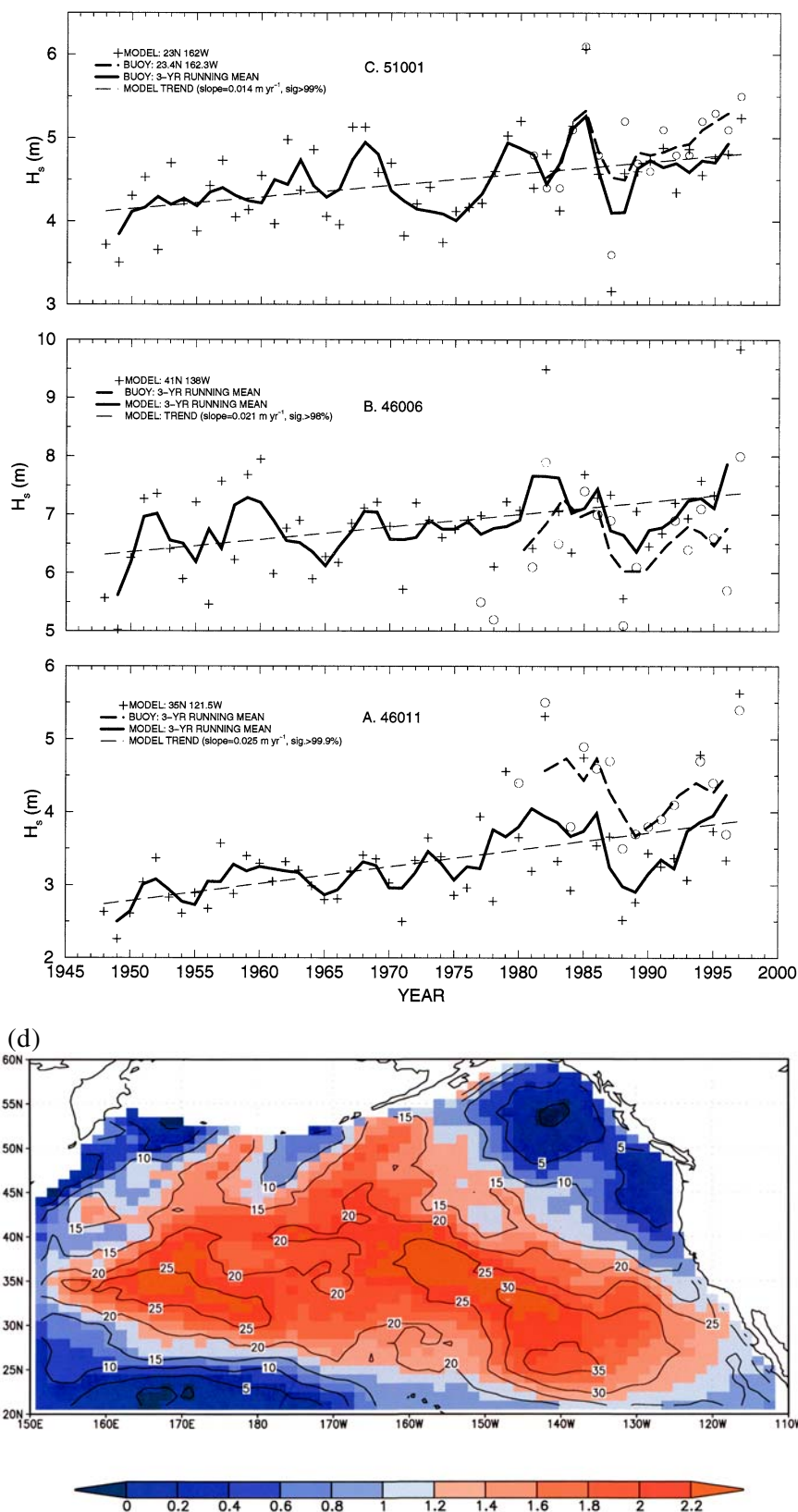


FIG. 11. Dec–Mar 95th percentile significant wave heights for NOAA buoys (a) 46011, (b) 46006, and (c) 51001; heavy solid and dashed lines are 3-yr running averages from hindcast and measured data, respectively; symbols are unsmoothed values; thin dashed lines show linear trends in hindcast data. For years with observations, the plotted data are for contemporaneous 3-hourly data. Buoy 46011 is located at 34.9°N, 120.9°W; the model grid point is at 35°N, 120°W. Buoy 46006 is located at 40.9°N, 137.5°W; model data grid point is at 41°N, 138°W. Buoy 51001 is located at 23.4°N, 162.3°W; model data grid point is at 23°N, 162°W. See Fig. 12a for locations. (d) Trends in hindcast Dec–Mar 99th percentile H_s [m (50 yr)⁻¹]. Black contour lines show trend expressed as a fraction of the long-term mean.

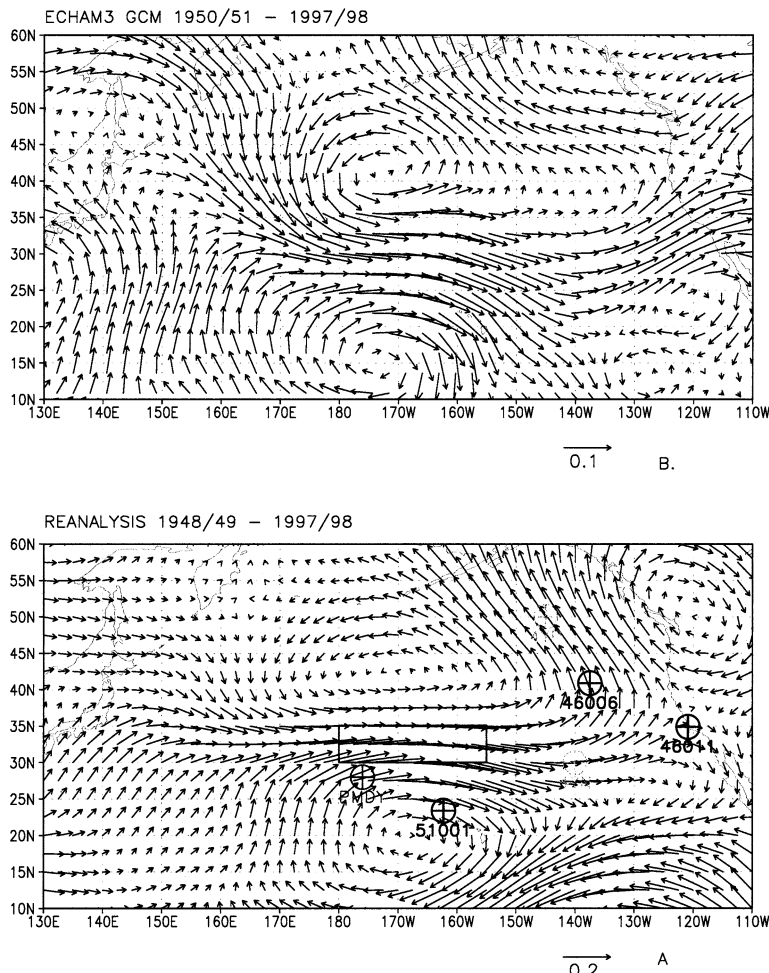


FIG. 12. Linear trends in 200-hPa winds from (a) reanalysis data (1948–97) and (b) the ECHAM3 AGCM (average of an ensemble of 10 simulations; 1950–97), using prescribed observed SSTs as forcing. Locations described in text are shown in (a).

of the midlatitude northeast Pacific south of 40°N, representing increases of 20%–35% when compared with the mean value (40%–70% in terms of wave energy). Along the coast of North America, the largest trends in hindcast extreme wave height (about 1 m) are found in southern California and southward into Baja California. (Note: an effort was made to use the COADS ship wave reports for this work. Because of reporting code changes instituted during the 1960s, the available wave data were not usable for long-term analysis. Further work is under way to rectify this situation.)

These findings have important implications for maritime operations, nearshore engineering, and coastal processes. The results also support earlier conjectures of increasing waves in the northeast Pacific based on both reconstructions of extreme-wave epi-

odes and more recent measured data (e.g., Strange and Graham 1982, 1999; Seymour 1996; Inman and Jenkins 1997; Allen and Komar 2000). From another perspective, these findings present an engaging counterpoint to the ongoing debate concerning the reality and significance of increasing waveheights in the North Atlantic (e.g., Carter and Draper 1988; Bacon and Carter 1991, 1993; Bouws et al. 1996; Kushnir et al. 1997; WASA Group 1998).

These wave analyses highlight the potential value of historical wave data to assist in documenting climate variability (including extreme events) over the North Pacific. In this regard it has been demonstrated that seismic data from Berkeley, California, can be used to reconstruct accurately the wave spectra measured by NOAA buoys near San Francisco with high (hourly) resolution [see Bromirski et al. (1999) and Grevemeyer et al. (2000) for examples of microseismic wave climate reconstruction for the northeast Pacific and North Sea, respectively]. Seismic records for the Berkeley site extend back to approximately 1930, offering the potential to reconstruct the San Francisco wave climate over the five decades prior to the beginning of the measured wave record in the early 1980s. Such a reconstruction would allow verification of some of the changes seen in

the reanalysis and wave hindcast data and would provide a unique record of North Pacific winter storm activity through much of the twentieth century.

4. Summary and discussion

Taken together, the results of this study portray a surprisingly regular and statistically significant pattern of increasingly vigorous wave cyclone activity across much of the North Pacific since the mid-twentieth century. During this time, the frequency of deep lows has increased by approximately 50%, minimum central pressures have declined by 4–5 hPa, and cyclone-associated extreme winds and relative vorticity have increased on the order of 10%–15%. In space, the reanalysis data show widespread negative trends in ex-

treme low SLP centered over central North Pacific, with a coherent pattern of increasing eddy activity (up to 30%) and westerly winds ($5\text{--}10\text{ m s}^{-1}$ in 50 yr) between 30° and 40°N , and rotation in the preferred direction of extreme winds from northwest to southwest in the Gulf of Alaska. Wave hindcast results show that, if the changes in the reanalysis winds are correct, the wave climate over much of the North Pacific has become much rougher since the 1950s, with extreme wave heights increasing on the order of $1\text{--}2\text{ m}$ (20%–30% of the long-term mean).

Comparisons with the relatively small amount of available in situ data (from OSVs, Midway Island radiosonde data, COADS, and SSTs) allow some verification of the changes seen in the reanalysis results. These comparisons support the downward trends in extreme SLP in the eastern North Pacific (VOS, 4YP, and 4YN), upward trends in rms SLP variability (Midway Island and 4YN), upward trends in zonal winds in the central Pacific (4YN, Midway Island, COADS, SSTs), and changes in preferred wind direction during high-wind events (4YP). Comparisons of extreme-wave statistics from buoy measurements and from the wave-model hindcast attest to the quality of the reanalysis winds during the last 20 yr of the record. The reality of the upward trends in wave heights through the rest of the hindcast record is supported by in situ and VOS wind and SLP records and is consistent with the downward trends in central North Pacific SSTs.

What is perhaps most interesting about the changes described above is the sense that they are associated with slow changes in background conditions rather than episodic forcing and appear to be largely unrelated to any increase in the frequency of El Niño episodes. It is not clear to what degree the changes in cyclone activity are related to a “Pacific decadal oscillation” [PDO; an index of low-frequency circulation variability in the North Pacific; Mantua et al. (1997)]. However, like many of the records shown here, the PDO has trended irregularly downward since the late 1940s and also exhibits some similarities at 10–20-yr timescales.

The trends found in our results have not been noted in other investigations of secular change in North Pacific cyclone climatology (e.g., Blackmon 1976; Wallace et al. 1988; Anderson and Gyakum 1989; Gyakum et al. 1989; Lau 1988; Rogers 1990). These studies used various indices of cyclone activity (eddy variability in midtropospheric heights, cyclone frequencies, and densities). The datasets used for these studies ranged from 8 to 30 yr in length and were de-

rived from (nonhomogeneous) numerical analyses, manually plotted synoptic charts, or cyclone track data. These studies emphasized three main findings broadly consistent with our results. These include (a) the presence of substantial year-to-year variability in the location of preferred cyclone tracks, cyclone frequency, and eddy variance; (b) the variability in cyclone behavior being related to lower-frequency changes in the atmospheric circulation; and (c) only modest association between cyclone and storm track characteristics with ENSO. It is interesting that the trends shown in our results were apparently foreshadowed in one of these studies (Anderson and Gyakum 1989; see their Fig. 6, middle panel). Whatever the case, given the quality of the available data and the relatively short duration and timing of the records, it is not surprising that secular trends were not detected. Recently, Key and Chan (1999) examined cyclone frequencies (without regard for central pressure) on the 1000- and 500-hPa constant pressure surfaces using NCEP reanalysis results from 1958 to 1997. The results, reported as aggregate statistics for the entire Northern Hemisphere midlatitudes, show a decrease in the number of December–February cyclones at 1000 hPa and an increase at 500 hPa. It is not clear whether their results are at odds with those reported here, in that the region covered, methodologies, and reported statistics are different. However, their results for the Northern Hemisphere midlatitude 500-hPa surface show trends and decadal variability not unlike the patterns seen in our results. (Note: 2–6-day band-passed SLP averaged over the entire midlatitude Northern Hemisphere for December–March shows a slight upward trend.)

If winter North Pacific cyclones have intensified, what is the cause? The evolution of baroclinic eddies (midlatitude cyclones) is a process in which potential energy contained in the background circulation, principally in the form of wind shear and temperature gradients, is converted to kinetic energy (e.g., Charney 1947; Eady 1949; Holopainen 1983; James 1994). The link between increasing upper-level westerlies and amplified cyclone activity is consistent with the idea that although eddies (cyclones) modify and can amplify the background upper-tropospheric circulation, the latter is most important in initiating eddy formation and controlling intensification (Held et al. 1989; Hoerling and Ting 1994; Trenberth and Hurrell 1994; Hurrell and van Loon 1997; Whitaker and Sardeshmukh 1998). Thus, a reasonable hypothesis is that the intensification of North Pacific winter cyclones has resulted from the increasing upper-tropospheric zonal winds

between 25° and 40°N. The similarity between the upper-level wind records (Fig. 10a) and the records of extreme and rms SLP (Figs. 5b, 6c–e, and 8) supports this idea. The broad spatial scale of the changes in upper-level winds can be appreciated in Fig. 12a, which shows trends in reanalysis winter mean 200-hPa winds. If these trends are at least qualitatively correct (as is supported by the data intercomparisons), slow changes in background conditions have provided an increasingly favorable environment for cyclone intensification. Such changes would also provide a mechanism for modulation of the response of the winter circulation over the North Pacific to interannual disturbances such as El Niño at decadal and longer timescale (e.g., Mantua et al. 1997; Gershunov et al. 1999; Dettinger et al. 2000).

What then has produced the upward trends in upper-level winds? One possibility is changes in tropical SSTs and resulting changes in organized tropical convection. Studies with models covering a wide range of complexity show that changes in the upper-level flow over the North Pacific similar to those observed on interannual-to-interdecadal timescales can be produced by low-frequency changes in tropical SSTs (e.g., Hoskins and Karoly 1981; Hoerling and Ting 1994; Lau 1997). These circulation changes result most directly not from the altered SSTs themselves but from ensuing increases in tropospheric heating due to enhanced organized deep convection (Hoskins and Karoly 1981; Ting and Held 1990; Ting and Hoerling 1993; Hoerling and Ting 1994; Lau 1997). Upper-level outflow from regions of tropical convection can interact with the background flow in the midlatitudes. These interactions can result in the redistribution and concentration of vorticity, with resulting changes in the favored configurations of the long waves in the upper-level westerlies [possibly with further modifications and feedbacks by with eddies and topography (e.g., Nigam and DeWeaver 1998)]. Such a scenario is at least plausible in this case.

The assimilation of observations into the model fields, changes in observational networks, and wide disparities between the spatial coverage of observations in the midlatitudes and Tropics makes direct diagnosis and attribution of this scenario using the reanalysis data problematic. However, the role of SSTs in producing the observed upper-level wind changes is supported by the trends in December–March 200-hPa winds for 1950–97 from the ECHAM3 AGCM simulation forced with observed SSTs (Fig. 12b). Although there are differences between the reanaly-

sis (Fig. 12a) and AGCM trend maps, the dominant features in each are the cyclonic–anticyclonic couplet located along 170°W and the region of increasing westerlies between. The resemblance between the behavior of the simulated and reanalysis upper-level winds is further supported by the time series of 200–850-hPa zonal wind shear from the AGCM shown in Fig. 10b (area average for 20°–35°N and 180°–150°W). The trend in the AGCM wind shear is approximately the same as in the reanalysis data ($0.11 \text{ m s}^{-1} \text{ yr}^{-1}$, significant above the 99% level) and is also in good agreement with the reanalysis and Midway records with regard to decadal variability.

The similarities in the reanalysis and simulated 200-hPa wind trends (Figs. 10b and 12) suggest that the changes in upper-level circulation over the North Pole resulted from changes in SST. Although it is not possible at this point to attribute these changes to SSTs in any particular region, there is some evidence that increasing SSTs in the tropical western Pacific may have been a factor in producing the observed upper-level trends over the North Pacific. As shown in Fig. 10b, the record of December–March SST in the region 20°S–5°N and 150°E–180° is remarkably similar to the upper-level wind and wind shear records for the North Pacific described earlier. This result is not especially sensitive to the region of the western tropical Pacific or eastern Indian Ocean used for averaging, so it is plausible that the general warming in this area has played a role in altering the behavior of North Pacific winter cyclones. On the other hand, these similarities in SSTs and North Pacific upper-level winds may be coincidental or might reflect some other underlying mechanism affecting both records. Further modeling and diagnostics studies may clarify this issue.

The question of a potential relationship between the cyclone intensification and anthropogenic greenhouse warming also arises. In this regard, most studies of midlatitude cyclone climatology in equilibrium greenhouse warming simulations suggest either little change or declining activity (Branscome and Gutowski 1992; Hall et al. 1994; Beersma et al. 1997; Zhang and Wang 1997). This decline has generally been ascribed to the reduced equator-to-pole temperature gradient and associated slackening of the upper-level westerlies. At the same time, some of these simulations do show localized regions of increased upper-level winds and eddy activity near the downstream ends of the principal storm tracks (e.g., Hall et al. 1994). Given the differences between various models (e.g., resolu-

tion, bias) and their results, it is not possible at this point to relate these simulated changes to those found in the reanalysis results. In contrast to the equilibrium greenhouse simulation results, some transient simulations with coupled ocean–atmosphere models do show an intensification and expansion of the Aleutian low during the latter decades of the twentieth century and early decades of the twenty-first century. These include the simulations described by Roeckner et al. [(1996); analysis by the authors using data available from <http://www.dkrz.de>],¹ Meehl and Washington (1996), and, more recently, Cai and Whetton (2000) and W. Cai and P. Whetton (2000, personal communication). In these simulations, the intensification of the Aleutian low may reflect differential rates of tropospheric warming between the tropical Indo–Pacific and midlatitude Pacific, with resulting increases in upper-level winds and increasing cyclone activity. Under this speculative scenario, an intensification of Pacific winter cyclones could be a transient phenomenon in which the more vigorous cyclone activity initially cools midlatitude SSTs through enhanced air–sea fluxes and turbulent mixing (e.g., Fig. 10b; see Miller et al. 1994; Deser et al. 1996), thus countering any radiative warming tendency (Cai and Whetton 2000). [At the same time, it should be noted that simulating systematic and reproducible impacts of midlatitude Pacific SST anomalies on the winter circulation has proved elusive (e.g., Peng et al. 1997; Blade 1997), arguing against a major active role of midlatitude SSTs in the observed changes.] Last, the observed intensification may be a manifestation of natural climate variability, and the mechanisms described above may be completely unrelated to the observed changes. In any case, further research is warranted concerning the verification, description, and genesis of the trends in winter cyclone climatology over the North Pacific.

Acknowledgments. This work was funded in part by the NOAA Climate Diagnostics Center (CDC), the Director’s Office of the Scripps Institution of Oceanography (SIO), Pacific Weather Analysis (PWA; Santa Barbara, California), and the Hydrologic Research Center. Many people assisted in various ways with this

¹Note that other recent transient coupled GCM simulations do not show an intensified Aleutian low and, in some cases, show the opposite (the character of changes in tropical Indo–Pacific SSTs is likely an important factor in this regard). Hence, agreement with the particular models is noted here only to suggest the possibility that the observed evolution of the winter cyclone climatology over the North Pacific could be at least partly be the result of greenhouse warming.

work. Thanks especially to Marty Hoerling for many valuable suggestions and ideas and thanks for suggestions and comments from Simon Mason, Mike Dettinger, Kosta Georgakakos, Ron Flick, Peter Bromirski, Doug Inman, and Scott Jenkins. Three reviewers provided thoughtful suggestions that resulted in substantial improvements in the manuscript. The initial ideas for this work grew out of long collaborations concerning extreme-wave reconstructions for California with R. Rea Strange of PWA. We thank Scott Woodruff and his team for providing the ocean weather ship data and Dian Seidel and Rebecca Ross (NOAA Air Resources Laboratory) for providing the Midway radiosonde data; these datasets were essential to the analysis. The ECHAM3 AGCM was developed at the Max Planck Institute for Meteorology at the University of Hamburg and was kindly provided by Lennart Bengtsson. The simulations with ECHAM3 were conducted by Mary Tyree of SIO. The WAVEWATCH III wave model was provided by the NOAA Ocean Modeling Branch and was implemented with assistance and advice from Hendrik Tolman. Pacific Weather Analysis funded and supplied the computer facilities for the wave modeling and purchased the reanalysis wind data. All other reanalysis data were obtained from CDC archives (<http://cdc.noaa.gov>), as were the COADS data.

References

- Allen, J., and P. Komar, 2000: Are ocean wave heights increasing in the eastern North Pacific? *Eos, Trans. Amer. Geophys. Union*, **81**, 561–567.
- Anderson, J. R., and J. R. Gyakum, 1989: A diagnostic study of Pacific basin circulation regimes as determined from extratropical cyclone tracks. *Mon. Wea. Rev.*, **117**, 2672–2686.
- Bacon, S., and D. J. T. Carter, 1991: Wave climate changes in the North Atlantic and North Sea. *Int. J. Climatol.*, **11**, 545–558.
- , and —, 1993: A connection between mean wave height and atmospheric pressure gradient in the North Atlantic. *Int. J. Climatol.*, **13**, 423–436.
- Beamish, R. J., and D. R. Bouillon, 1993: Pacific salmon production trends in relation to climate. *Can. J. Fish Aquat. Sci.*, **50**, 1002–1016.
- Beersma, J. J., K. M. Rider, G. J. Komen, E. Kaas, and V. V. Kharin, 1997: An analysis of extra-tropical storms in the North Atlantic region as simulated in a control and $2 \times \text{CO}_2$ time-slice experiment with a high-resolution atmospheric model. *Tellus*, **49A**, 347–361.
- Bengtsson, L., U. Schlese, E. Roekner, M. Latif, T. P. Barnett, and N. E. Graham, 1993: A two-tiered approach to long-range climate forecasting. *Science*, **261**, 1026–1028.
- Bitz, C. M., and D. S. Battisti, 1999: Interannual to decadal variability in climate and the glacier mass balance in Washington, western Canada, and Alaska. *J. Climate*, **12**, 3181–3196.
- Bjerknes, J., 1966: A possible response of the atmospheric Hadley circulation to equatorial anomalies in ocean temperature. *Tellus*, **18**, 820–829.
- Blackmon, M. L., 1976: A climatological spectral study of the 500-mb geopotential height of the Northern Hemisphere. *J. Atmos. Sci.*, **33**, 1607–1623.
- Blade, I., 1997: The effects of midlatitude ocean–atmosphere coupling on the low-frequency variability of a general cir-

- lation model. Part I: No tropical forcing. *J. Climate*, **10**, 2087–2106.
- Bouws, E., D. Jannick, and G. J. Komen, 1996: The increasing wave height in the North Atlantic Ocean. *Bull. Amer. Meteor. Soc.*, **77**, 2275–2277.
- Branscome, L. E., and W. J. Gutowski, 1992: The impact of doubled CO₂ on the energetics and hydrologic processes of mid-latitude transient eddies. *Climate Dyn.*, **8**, 29–37.
- Bromirski, P. D., R. E. Flick, and N. Graham, 1999: Ocean wave height determined from inland seismometer data: Implications for investigating wave climate changes. *J. Geophys. Res.*, **104**, 20 753–20 766.
- Cai, W., and P. H. Whetton, 2000: Evidence for a time-varying pattern of greenhouse warming in the Pacific Ocean. *Geophys. Res. Lett.*, **27**, 2577–2580.
- Cardone, V. J., J. G. Greenwood, and M. A. Cane, 1990: On trends in historical marine wind data. *J. Climate*, **3**, 113–127.
- Carter, D. J. T., and L. Draper, 1988: Has the north-east Atlantic become rougher? *Nature*, **332**, 494.
- Cayan, D. R., and D. H. Peterson, 1989: The influence of North Pacific circulation on streamflow in the west. *Aspects of Climate Variability in the Pacific and Western Americas*, *Geophys. Monogr.*, No. 55, Amer. Geophys. Union, 365–374.
- , A. J. Miller, T. P. Barnett, N. E. Graham, J. N. Ritchie, and J. M. Oberhuber, 1993: Seasonal–interdecadal fluctuations in surface temperature over the Pacific: Effects of monthly winds and heat fluxes. *Natural Climate Variability on Decadal-to-Century Time Scales*, W. A. Sprigs, Ed., National Academy Press, 133–150.
- Charney, J. G., 1947: The dynamics of long waves in a westerly baroclinic current. *J. Meteor.*, **4**, 135–163.
- Deser, C., M. A. Alexander, and M. Timlin, 1996: Upper ocean thermal variations in the North Pacific during 1970–91. *J. Climate*, **9**, 1840–1855.
- Dettinger, M. D., and D. R. Cayan, 1995: Large-scale of recent trends toward early snowmelt runoff in California. *J. Climate*, **8**, 606–623.
- , D. S. Battisti, R. D. Garreaud, G. J. McCabe, and C. M. Bitz, 2000: Interhemispheric effects of interannual and decadal ENSO-like climate variations in the Americas. *Interhemispheric Climate Linkages*, V. Markgraf, Ed., Academic Press, 1–16.
- Diaz, H. F., X. Quan, and C. Fu, 1994: Marine surface wind changes during 1978–1992: An estimation based on COADS. *Proc. Int. COADS Winds Workshop*, Kiel, Germany, NOAA and Inst. für Meereskunde, 48–67.
- DKRZ, 1992: The ECHAM3 atmospheric general circulation model. Tech. Rep. 6, Deutsches Klimarechenzentrum, Hamburg, Germany, 184 pp.
- Eady, E. T., 1949: Long waves and cyclone waves. *Tellus*, **1**, 33–52.
- Gershunov, A., T. P. Barnett, and D. R. Cayan, 1999: North Pacific interdecadal oscillations seen as factor in ENOS-related North American climate anomalies. *Eos, Trans. Amer. Geophys. Union*, **80**, 24, 29–30.
- Graham, N. E., 1994: Decadal-scale climate variability in the tropical and North Pacific during the 1970s and 1980s: Observations and model results. *Climate Dyn.*, **10**, 135–162.
- , T. P. Barnett, R. Wilde, M. Ponater, and S. Schubert, 1995: On the roles of tropical and midlatitude SSTs in forcing interannual and interdecadal variability in the winter Northern Hemisphere circulation. *J. Climate*, **7**, 1416–1441.
- , R. R. Strange, and H. F. Diaz, 2001: A 50-year winter wave hindcast of the North Pacific using NCEP/NCAR reanalysis winds. in preparation.
- Grevenmeyer, I., R. Herber, and H.-H. Essen, 2000: Microseismological evidence for a changing wave climate in the northeast Atlantic Ocean. *Nature*, **408**, 348–353.
- Gyakum, J. R., J. R. Anderson, R. H. Grumm, and E. C. Gunner, 1989: North Pacific cold-season cyclone activity, 1975–1993. *Mon. Wea. Rev.*, **117**, 1141–1155.
- Hall, N. M. J., B. J. Hoskins, P. J. Valdes, and C. A. Senior, 1994: Storm tracks in a high-resolution GCM with doubled carbon dioxide. *Quart. J. Roy. Meteor. Soc.*, **120**, 1209–1230.
- Held, I. M., S. W. Lyons, and S. Nigam, 1989: Transients and the extratropical response during El Niño. *J. Atmos. Sci.*, **46**, 163–174.
- Hoerling, M. P., and M. Ting, 1994: Organization of extratropical transients during El Niño. *J. Climate*, **7**, 745–766.
- Holopainen, E. O., 1983: Transient eddies in the mid-latitudes: Observations and interpretation. *Large-Scale Dynamical Processes in the Atmospheres*, B. J. Hoskins and R. P. Pierce, Eds., Academic Press, 201–233.
- Hoskins, B. J., and D. J. Karoly, 1981: The steady linear response of a spherical atmosphere to thermal and orographic forcing. *J. Atmos. Sci.*, **38**, 1179–1196.
- Hurrell, J. W., and H. van Loon, 1997: Decadal variations in climate associated with the North Atlantic oscillation. *Climatic Change*, **36**, 301–326.
- Inman, D. L., and S. A. Jenkins, 1997: Changing wave climate and littoral drift along the California coast. *Proc. California and the World Ocean '97*, San Diego, CA, American Society of Civil Engineers, 538–549.
- Isemer, H.-J., 1994: Trends in marine surface wind speed: Ocean weather stations versus voluntary observing ships. *Proc. Int. COADS Winds Workshop*, Kiel, Germany, NOAA and Inst. für Meereskunde, 68–84.
- James, I. N., 1994: Interaction between transient and steady eddies. *Introduction to Circulating Atmospheres*, Cambridge University Press, 220–242.
- Kalnay, E., and Coauthors, 1996: The NCEP/NCAR 40-Year Reanalysis Project. *Bull. Amer. Meteor. Soc.*, **77**, 437–471.
- Key, K. R., and A. C. K. Chan, 1999: Multidecadal global and regional trends in 1000 mb and 500 mb cyclone frequencies. *Geophys. Res. Lett.*, **26**, 2053–2056.
- Kushnir, Y., V. J. Cordone, and J. G. Greenwood, 1997: The recent increase in North Atlantic wave heights. *J. Climate*, **10**, 2107–2113.
- Latif, M., and T. P. Barnett, 1994: On the causes of decadal climate variability over the North Pacific and North America. *Science*, **266**, 634–637.
- Lau, N.-C., 1988: Variability in the observed midlatitude storm tracks in relation to low-frequency changes in the circulation pattern. *J. Atmos. Sci.*, **45**, 2718–2743.
- , 1997: Global SST anomalies and the midlatitude atmospheric circulation. *Bull. Amer. Meteor. Soc.*, **78**, 21–33.
- Lomb, N. R., 1976: Least squares frequency analysis of unequally spaced data. *Astrophys. Space Science*, **391**, 447–462.
- Mantua, N. J., S. R. Hare, Y. Zhang, J. M. Wallace, and R. C. Francis, 1997: A Pacific interdecadal oscillation with impacts on salmon production. *Bull. Amer. Meteor. Soc.*, **78**, 1069–1079.

- Meehl, G. A., and W. M. Washington, 1996: El Niño-like climate change in a model with increased atmospheric CO₂ concentrations. *Nature*, **382**, 56–60.
- Miller, A. J., D. R. Cayan, T. P. Barnett, N. E. Graham, and J. M. Oberhuber, 1994: Interdecadal variability of the Pacific Ocean: Model response to observed heat flux and wind stress anomalies. *Climate Dyn.*, **9**, 287–302.
- Nigam, S., and E. DeWeaver, 1998: Influence of orography on the extratropical response to El Niño events. *J. Climate*, **11**, 716–733.
- Nitta, T., and S. Yamada, 1989: Recent warmings in tropical sea surface temperature and its relationship to the Northern Hemisphere circulation. *J. Meteor. Soc. Japan*, **67**, 375–383.
- Overland, J. E., S. Salo, and J. M. Adams, 1999: Salinity signatures of the PDO. *Geophys. Res. Lett.*, **26**, 1337–1340.
- Peixoto, J. P., and A. H. Oort, 1992: *The Physics of Climate*. American Institute of Physics, 496 pp.
- Peng, S., W. A. Robinson, and M. P. Hoerling, 1997: The modeled atmospheric response to midlatitude SST anomalies and its dependence on the background circulation state. *J. Climate*, **10**, 971–987.
- Polovina, J. J., G. T. Mitchum, and G. T. Evans, 1995: Decadal and basin-scale variations in mixed layer depths and impact on biological production in the central and North Pacific. *Deep-Sea Res.*, **42**, 1701–1716.
- Press, W. H., and G. B. Rybicki, 1989: Fast algorithm for spectral analysis of unevenly sampled data. *Astrophys. J.*, **338**, 277–280.
- , S. A. Teukolsky, W. T. Vetterling, and B. P. Flannery, 1992: *Numerical Recipes in C: The Art of Scientific Computing*. 2d ed. Cambridge University Press, 994 pp.
- Roeckner, E., J. M. Oberhuber, A. Bacher, M. Christoph, and I. Kircher, 1996: ENSO variability and atmospheric response in a global coupled atmosphere–ocean GCM. *Climate Dyn.*, **12**, 737–754.
- Roemmich, D., and J. McGowen, 1995: Climate warming and the decline of zooplankton in the California Current. *Science*, **267**, 1324–1326.
- Rogers, J. C., 1990: Patterns of low-frequency monthly sea level pressure variability (1899–96) and associated wave cyclone frequencies. *J. Climate*, **3**, 1364–1379.
- Ruggiero, P., G. M. Kaminsky, P. D. Komar, and W. G. McDougal, 1997: Extreme waves and coastal erosion in the Pacific Northwest. *Proceeding of Waves 97, the Third International Symposium on Ocean Wave Measurement and Analysis*, B. L. Edge and J. M. Hemsley, Eds., ASCE, 947–961.
- Scargle, J. D., 1982: Studies in astronomical time series analysis II. Statistical aspects of spectral analysis of unevenly spaced data. *Astrophys. J.*, **263**, 835–853.
- Seymour, R. J., 1996: Wave climate variability in southern California. *J. Waterway, Port, Coastal, Ocean Eng.*, **122**, 182–186.
- , R. R. Strange, D. R. Cayan, and R. A. Nathan, 1984: Influence of El Niños on California's wave climate. *Proc. 19th Int. Conf. on Coastal Engineering*, Houston TX, American Society of Coastal Engineers, 577–592.
- Sinclair, M. R., and I. G. Watterson, 1999: Objective assessment of extratropical weather systems in simulated climates. *J. Climate*, **12**, 3467–3485.
- Smith, T. M., R. W. Reynolds, R. E. Livezey, and D. C. Stokes, 1996: Reconstruction of historical surface temperatures using empirical orthogonal functions. *J. Climate*, **9**, 1403–1420.
- Strange, R. R., and N. E. Graham, 1982: Hindcast severe storm waves at Diablo Canyon, California. Pacific Weather Analysis, 43 pp. [Available from Pacific Weather Analysis, 648 Ladera Lane, Santa Barbara, CA 93106.]
- , and ———, 1999: Hindcast of extreme wave events at Guadalupe Oil Field, Santa Maria, California. Pacific Weather Analysis, 42 pp. plus appendices. [Available from Pacific Weather Analysis, 648 Ladera Lane, Santa Barbara, CA 93106.]
- , ——— and D. R. Cayan, 1989: Meteorological development of the unusually severe coastal storm during January 16–18, 1988. *Shore Beach*, **57**, 3–9.
- Ting, M.-F., and I. M. Held, 1990: The stationary wave response to a tropical SST anomaly in an idealized general circulation model. *J. Atmos. Sci.*, **47**, 2546–2566.
- , and M. P. Hoerling, 1993: The dynamics of stationary wave anomalies during the 1986/87 El Niño. *Climate Dyn.*, **9**, 147–164.
- Tolman, H. L., 1999: User manual and system documentation of WAVEWATCH III, version 1.18. Ocean Modeling Branch Contribution 166, NOAA/NWS/NCEP, 112 pp. [Available from NOAA/NWS/NCEP, 4700 Silver Hill Road, Mail Stop 9910, Washington, DC 20233-9910.]
- Trenberth, K. E., 1990: Recent observed interdecadal climate changes in the Northern Hemisphere. *Bull. Amer. Meteor. Soc.*, **71**, 998–993.
- , and J. W. Hurrell, 1994: Decadal atmosphere–ocean variations in the Pacific. *Climate Dyn.*, **9**, 303–319.
- , and D. A. Paulino, 1980: The northern hemisphere sea-level pressure data set: Trends, errors, and discontinuities. *Mon. Wea. Rev.*, **108**, 855–872.
- Venrick, E. L., J. A. McGowen, D. R. Cayan, and T. L. Hayward, 1987: Climate and chlorophyll a: Long-term trends in the central North Pacific. *Science*, **238**, 70–72.
- Wallace, J. M., and D. S. Gutzler, 1983: Teleconnections in the geopotential height field during Northern Hemisphere winter. *Mon. Wea. Rev.*, **109**, 784–812.
- , G.-H. Lim, and M. Blackmon, 1988: Relationships between cyclone tracks, anti-cyclone tracks, and baroclinic waveguides. *J. Atmos. Sci.*, **45**, 439–462.
- Ward, N. M., 1992: Provisionally corrected surface wind data, worldwide ocean–atmosphere surface fields, and Sahelian rainfall variability. *J. Climate*, **5**, 454–475.
- , 1994: Near-surface wind, SLP, and SST: Some interrelationships and a set of corrections for wind trends 1949–88. *Proc. COADS Winds Workshop*, Kiel, Germany, NOAA and Inst. für Meereskunde, 102–119.
- , and B. J. Hoskins, 1996: Near-surface wind over the global ocean 1949–88. *J. Climate*, **9**, 1877–1895.
- WASA Group, 1998: Changing waves and storms in the northeast Atlantic. *Bull. Amer. Meteor. Soc.*, **79**, 741–761.
- Whitaker, J. S., and P. D. Sardeshmukh, 1998: A linear theory of extratropical synoptic eddy statistics. *J. Atmos. Sci.*, **55**, 237–258.
- Woodruff, S. D., R. J. Slutz, R. L. Jenne, and P. M. Steurer, 1987: A comprehensive ocean–atmosphere data set. *Bull. Amer. Meteor. Soc.*, **68**, 1239–1250.
- Zhang, Y., and W.-C. Wang, 1997: Model-simulated northern winter cyclone and anticyclone activity under a greenhouse warming scenario. *J. Climate*, **10**, 1616–1636.
- , J. M. Wallace, and D. S. Battisti, 1997: ENSO-like interdecadal variability: 1900–93. *J. Climate*, **10**, 1004–1020.